Light scattering in a phonon gas

Akitoshi Koreeda, Ryuta Takano, and Seishiro Saikan
Department of Physics, Graduate School of Science, Tohoku University, Sendai 980-8578, Japan
(Received 2 March 2009; revised manuscript received 10 July 2009; published 2 October 2009)

Light-scattering spectrum in dielectric crystals is studied with extended thermodynamics (ET) for a phonon gas, covering from hydrodynamic to ballistic (collisionless) regimes. The ET equation is solved to obtain the power spectrum of the energy density in a phonon-gas mixture, which consists of interacting phonon gases of longitudinal and transverse acoustic (LA and TA) phonon modes. In the hydrodynamic regime, where phonon collisions take place frequently, it is found that the light-scattering spectrum consists of two components, which can be interpreted as the two normal modes formed by the two second-sound modes defined in each of the LA and TA phonon gases. Out of the two normal-mode spectra, the low-frequency component arises from thermal fluctuations and gives rise to a narrow quasielastic spectrum, which corresponds to the well-known thermal Rayleigh scattering due to thermal diffusion, i.e., due to overdamped second sound. With sufficient momentum-conserving phonon collisions (normal phonon scattering), the narrow quasielastic component is demonstrated to develop, from the diffusive central peak, into a pair of shifted inelastic peaks due to propagation of underdamped second sound. The other spectrum component gives rise to a much broader quasielastic scattering, whose wing extends out to the Brillouin-scattering lines of the LA and TA phonons (first sounds). The broader quasielastic spectrum has a linewidth equal to the phonon-collision rate, which suggests that this component originates from a nonequilibrium process in the phonon gas. As the ballistic regime is approached, the line shapes and linewidths of the two normal-mode spectra approach each other, and the two components finally coincide in the limit of the ballistic regime, which is in good agreement with the reported behavior for these spectra that were experimentally observed in many crystals. In the ballistic limit, the light-scattering mechanism in the present model is found to become formally equivalent to the previously proposed microscopic framework, i.e., the second-order difference Raman scattering (two-phonon difference light scattering) on a same phonon dispersion. The derived spectral formula is fitted to the spectra previously observed in the experiments for rutile (TiO_2) and strontium titanate ($SrTiO_3$). The fits are quite successful in wide ranges of frequency and temperature, i.e., regardless of degree of nonequilibrium, owing to the ET analysis. The relaxation times for the normal and resistive phonon collisions (τ_N and τ_R) are determined through the analysis. The temperature dependences of τ_N and τ_R indicate that the origin of the broad shifted peaks (the "broad doublet"), which were observed in $SrTiO_3$ at around 30 K, is likely due to underdamped second sound at least in a narrow temperature range around 30 K.

DOI: 10.1103/PhysRevB.80.165104 PACS number(s): 78.35.+c, 63.20.−e, 66.30.Xj, 77.90.+k

I. INTRODUCTION

Transport phenomenon is a fundamental nonequilibrium aspect in many-body systems, where thermal equilibrium is realized through the interactions among constituent particles such as molecules, electrons, phonons, etc. One of the most important transport phenomena is the energy transport in dielectric solids, where the energy (or "heat") is carried only by phonons at a velocity of sound speed. Studying the energy transport in dielectric solids brings us understandings of the mechanism of thermal diffusion, wavelike propagation of heat ("second sound"), ballistic heat conduction.[1–3] In dielectric solids, the conduction of heat is realized through the lattice anharmonicity, which allows for collisions between phonons in a "phonon gas.[2,4]"

In early version of nonequilibrium physics that deals with dissipation including diffusion phenomena, it was essential to assume that thermal equilibrium is always achieved locally in a "small cell" of the relevant system.[5,6] Owing to this local-thermal-equilibrium hypothesis, local thermodynamic variables, such as local temperature, local entropy, etc., may be defined in the length scale of the small cells, and it is possible that the entire system is not necessarily in thermal equilibrium as a whole. For local thermal equilibrium to be achieved in the small cells, the mean free path of the energy quanta (such as molecules, phonons, electrons, etc.) in the cells must be sufficiently shorter than the dimension of the small cells; otherwise, we see the nonequilibrium kinetic behavior inside the individual cells. If the mean free path of the quanta is comparable to the observation length scale, the memory effect of successive collisions between the energy quanta should not be neglected. Since the mean free path of phonons in most dielectric solids can range from nm to μm or even to mm scales as the temperature is reduced, we cannot always assume local thermal equilibrium within a fixed length scale. Therefore, it is possible that local thermal equilibrium is violated due to temperature change. If local thermal equilibrium is violated, we must consider the correlation between the phonon collisions: such process involves frequency and wave-vector dependences of the transport coefficients such as thermal conductivity or diffusivity.

We have recently reported on light-scattering experiments in crystals of rutile, ZnSe, silicon, and $SrTiO_3$.[7] We found that, at relatively high temperatures, the low-frequency part of the light-scattering spectra consisted of two quasielastic components. Out of the two quasielastic components, the narrower component broadened on cooling, and it had a line-

width that could be well reproduced as $D_{\mathrm{th}}q^2$ at high temperatures, where D_{th} is the thermal diffusivity and q is the wave-vector transfer in the experiments. However, the observed linewidth of the narrower quasielastic component did not follow $D_{\mathrm{th}}q^2$ at low temperatures, showing that the observation length scale of q^{-1}, which was $\lesssim 100$ nm, was too short compared to the mean free path of phonons,[7] which becomes longer at low temperature because the number of the thermally excited phonons decreases as the temperature is lowered. The other quasielastic component, the broader one, showed opposite temperature dependence for the linewidth, i.e., it narrowed on cooling, and had no q dependence; therefore, the two quasielastic components approached each other on cooling. However, we could not quantitatively analyze such a behavior in the low-temperature region due to the lack of theories that cover the whole temperature range. In $SrTiO_3$, it has been reported by Hehlen *et al.*[8] that an extra soundlike peak appears in the Brillouin-scattering spectrum around 30 K, and they tentatively ascribed the extra Brillouin peak to the second sound, the wavelike propagation of heat,[2] basing on a theoretical work by Gurevich and Tagantsev.[9] We found that the extra Brillouin spectrum was seemingly developed from the thermal-diffusive (the narrow) quasielastic component. Since thermal diffusion is considered as overdamped second sound,[10–12] the spectrum of second sound should transform gradually from a quasielastic profile into a pair of shifted peaks as the thermal wave becomes underdamped. However, in order to deal with all of the above aspects of the low-frequency light-scattering spectra (thermal diffusion, second sound, nonequilibrium heat transport, the broader quasielastic component, etc.), it is essential to formulate the nonequilibrium light-scattering theory that can be applied not only when local thermal equilibrium can be assumed but also when it cannot be established.

Recently, a method of nonequilibrium thermodynamics has been developed,[5] and it has succeeded in reproducing the pressure dependence of the light-scattering spectrum in rarefied gases. Also, thermal diffusion, propagation of second sound, and ballistic phonon propagation in NaF (Ref. 13) has been well simulated from relatively simple formalism with phonon-gas model.[5,6,14] Although the theoretical framework that is called "extended thermodynamics (ET)" seems to be still under test, it is becoming a powerful tool for the analysis of experimental data that concerns highly nonequilibrium processes.[5,6]

In this paper, we solve a set of ET equations for a phonon-gas system to obtain the formula for the light-scattering spectra that is applicable from equilibrium to nonequilibrium regimes in dielectrics. In Sec. II, the derivation of the spectral formula is presented. The narrow central peak due to thermal diffusion (thermal Rayleigh mode), the broad Brillouin doublet due to second sound, and the broad central peak (Mountain mode in crystals) are discussed in that section. Also, we discuss how the nonequilibrium energy-transport affects those "equilibrated" spectra when the nonequilibrium is approached. In Sec. III, we fit the derived expression to the experimentally observed spectra for rutile and $SrTiO_3$ crystals. The possibility of second sound in these systems is discussed in Sec. IV, and it is concluded that the reported broad doublet in $SrTiO_3$ (Ref. 8) is likely due to second sound. Finally, we summarize this report in Sec. V.

II. THEORY

A. Extended thermodynamic equations for a mixture of phonon gases

In order to realistically characterize the phonon gas in a dielectric, we consider the anharmonic interactions between different phonon modes, namely, longitudinal and transverse acoustic (LA and TA) modes, rather than considering only a single phonon mode. Following the treatments in the review by Dreyer and Struchtrup,[5,14] who have carried out ET analyses on boson gases, the ET equations to be solved is given as follows for *one-dimensional* case:[14]

$$\frac{\partial e^{(l)}}{\partial t} + c_{(l)}^2 \frac{\partial p_x^{(l)}}{\partial x} = -2A(c_{(l)}^3 e^{(l)} - c_{(t)}^3 e^{(t)}) \tag{1a}$$

$$\frac{\partial p_x^{(l)}}{\partial t} + \frac{1}{3}\frac{\partial e^{(l)}}{\partial x} + \frac{\partial N_{\langle xx\rangle}^{(l)}}{\partial x} = -\frac{1}{\tau_{\mathrm{R}}^{(l)}} p_x^{(l)} - 2B(c_{(l)}^5 p^{(l)} - c_{(t)}^5 p^{(t)}) \tag{1b}$$

$$\vdots$$

$$\frac{\partial u_{\langle n-1\rangle}^{(l)}}{\partial t} + \alpha_n c_{(l)}^2 \frac{\partial u_{\langle n-2\rangle}^{(l)}}{\partial x} + \frac{\partial u_{\langle n\rangle}^{(l)}}{\partial x} = -\left(\frac{1}{\tau_{\mathrm{N}}^{(l)}} + \frac{1}{\tau_{\mathrm{R}}^{(l)}}\right) u_{\langle n-1\rangle}^{(l)} \tag{1c}$$

$$\frac{\partial e^{(t)}}{\partial t} + c_{(l)}^2 \frac{\partial p_x^{(t)}}{\partial x} = A(c_{(l)}^3 e^{(l)} - c_{(t)}^3 e^{(t)}) \tag{2a}$$

$$\frac{\partial p_x^{(t)}}{\partial t} + \frac{1}{3}\frac{\partial e^{(t)}}{\partial x} + \frac{\partial N_{\langle xx\rangle}^{(l)}}{\partial x} = -\frac{1}{\tau_{\mathrm{R}}^{(t)}} p_x^{(t)} + B(c_{(l)}^5 p^{(l)} - c_{(t)}^5 p^{(t)}) \tag{2b}$$

$$\vdots$$

$$\frac{\partial u_{\langle n-1\rangle}^{(t)}}{\partial t} + \alpha_n c_{(t)}^2 \frac{\partial u_{\langle n-2\rangle}^{(t)}}{\partial x} + \frac{\partial u_{\langle n\rangle}^{(t)}}{\partial x} = -\left(\frac{1}{\tau_{\mathrm{N}}^{(t)}} + \frac{1}{\tau_{\mathrm{R}}^{(t)}}\right) u_{\langle n-1\rangle}^{(t)}. \tag{2c}$$

Here, the traceless symmetric parts of a tensor of rank n, $T_{i_1\cdots i_n}$, are denoted by $T_{\langle i_1\cdots i_n\rangle}$, and further abbreviation such as $T_{\langle i_1\cdots i_n\rangle} \equiv T_{\langle n\rangle}$ is used.[5,14] The moments of the phase density (distribution function) f are defined by the equation[14]

$$u_{\langle n\rangle} \equiv u_{\langle i_1\cdots i_n\rangle} = \hbar \int \left(\frac{c}{k}\right)^{n-1} k_{\langle i_1} \cdots k_{i_n\rangle} f d\boldsymbol{k}.$$

For $n=0,1,2,\ldots$, we obtain $e^{(\lambda)}=c^2 u_{\langle 0\rangle}^{(\lambda)}$, $p^{(\lambda)}=u_x^{(\lambda)}=u_{\langle 1\rangle}^{(\lambda)}$, $N_{\langle xx\rangle}^{(\lambda)}=u_{\langle 2\rangle}^{(\lambda)},\ldots$, and $u_{\langle n\rangle}^{(\lambda)}=u_{\langle xx\cdots x_n\rangle}^{(\lambda)}$, which are, respectively, the energy density, the momentum density, the momentum flux (the traceless symmetric part of the stress tensor), …, and the general flux deviator of order n.[5,6,14] $(\lambda)=(l)$ or (t) denotes the phonon mode LA or TA, respectively. $c_{(\lambda)}$ is the sound velocity, and $\tau_{\mathrm{R}}^{(\lambda)}$ and $\tau_{\mathrm{N}}^{(\lambda)}$ are the relaxation times for the resistive (R) and normal (N) processes of phonon-phonon

scattering, respectively. Note that the R process include the Umklapp and other nonmomentum-conserving collisions between phonons, while the N process does not destroy momentum conservation. α_n is defined by

$$\alpha_n \equiv \frac{(n-1)^2}{4(n-1)^2-1}. \tag{3}$$

The coupling constants responsible for the exchanges of energy and momentum between the two sound modes are defined, respectively, by

$$A = \frac{1}{\tau_{\mathrm{R}}^{(t)} c_{(t)}^3 + 2\tau_{\mathrm{R}}^{(l)} c_{(l)}^3} + \frac{1}{\tau_{\mathrm{N}}^{(t)} c_{(t)}^3 + 2\tau_{\mathrm{N}}^{(l)} c_{(l)}^3}, \tag{4}$$

$$B = \frac{1}{\tau_{\mathrm{N}}^{(t)} c_{(t)}^5 + 2\tau_{\mathrm{N}}^{(l)} c_{(l)}^5}. \tag{5}$$

The set of Eqs. (1a) and (2c) consists of $2n$ equations, i.e., n balance equations for the "fields" for each of the modes. Each equation is obtained from the Boltzmann equation multiplied by $u_{\langle n\rangle}$ and then integrated over the whole Brillouin zone, combined with Callaway's relaxation-time approximation,[15] which assumes two relaxation times, τ_{N} and τ_{R}. Equation (1a), the first balance equation for the LA mode, is a continuity equation for the energy density with a production term (the right-hand side) due to the interaction with the other modes (two TA modes). The total energy $e = e^{(l)} + 2e^{(t)}$ is conserved, but there is an exchange of energy between the modes unless $c_{(l)}^3 e^{(l)} - c_{(t)}^3 e^{(t)} = 0$ holds. Due to N processes, there is an exchange of momentum between the modes unless $c_{(l)}^5 p_x^{(l)} - c_{(t)}^5 p_x^{(t)} = 0$.

In this ET model, we consider all the phonons in the whole Brillouin zone, i.e., not only the long-wavelength phonons but also those with much shorter wavelength (much larger wave vectors).[14] It should be pointed out that the phonon lifetime is shorter for phonons with larger wave vectors. Therefore, phonon collisions within one branch as well as those between different branches can be considered in this model. The intramode phonon collision is expected to occur far less frequently in crystals[16] if one neglects the life time of thermal phonons (i.e., in the ballistic regime), but, in general, one should include not only the intermode but also the intramode phonon collisions in order to account for the collective excitations in a phonon gas. Another remark is that the one-dimensional model assumes that the phonons traveling in all the directions can participate in the collisions.

B. Light scattering in phonon gas

Light scattering occurs through the modulation in dielectric constant ϵ by the fluctuations in the thermodynamic variables such as the density or temperature in the medium. In Landau-Placzek theory,[17] the fluctuation in ϵ is described by the following relation:

$$\delta\epsilon = \left(\frac{\partial\epsilon}{\partial\rho}\right)_T \delta\rho + \left(\frac{\partial\epsilon}{\partial T}\right)_\rho \delta T, \tag{6}$$

where ρ and T are the density and temperature, respectively. In phonon picture, this is expressed equivalently as[18,19]

$$\delta\epsilon = p_1(\boldsymbol{q})A(\boldsymbol{q}) + \sum_q p_2(\boldsymbol{q}_1,\boldsymbol{q}_2)A(\boldsymbol{q}_1)A(\boldsymbol{q}_2), \tag{7}$$

where p_1 and p_2 are the first- and second-order Raman coefficients, respectively, and A is the phonon normal coordinate. p_1 gives (ordinary) one-phonon scattering (first-order Raman scattering), and p_2 gives second-order Raman scattering, where number-density fluctuations in the phonon gas is responsible for the light-scattering mechanism. The power spectrum, $\langle \delta\epsilon^* \delta\epsilon\rangle$, calculated from Eq. (6) and (7) contains three types of terms: (i) scattering from a single phonon; (ii) scattering from a pair of phonons; (iii) the interference between the contributions of (i) and (ii). In ordinary fluids, only the contribution of (i) is usually considered because the second contribution is much smaller than the first due to relatively large thermal-expansion effect, which indirectly connects the temperature change to the dielectric constant.[17] The Brillouin scattering from elastic sound wave originates from the contribution from the p_1 term, i.e., it is the first-order scattering in which a single phonon is relevant.

In contrast to light scattering in ordinary fluids, the second-order term, (ii), plays a significant role in solids, and it gives rise to light scattering directly due to thermal fluctuations, i.e., the dielectric constant is modulated directly (not via thermal-expansion effect) by the fluctuations in number density of phonons.[18] Since the number density of phonons is proportional to the energy density $[e(x,t)]$ in the phonon gas, its power spectrum, $\langle e^* e\rangle$, which we will calculate from the ET equations, describes only the contribution from the second term in the right-hand side of Eq. (7). The power spectrum, $\langle e^* e\rangle$, should not include the first-order scattering because it contains at least four phonon coordinates, and the Brillouin scattering from a sound wave will not appear in our calculated spectrum, which will be presented below. Since we have been interested in the quasielastic light scattering in solids, including thermal Rayleigh scattering or other low-energy scattering involving a collection of phonons, we will focus only on the second-order scattering, which can be described by the power spectrum of the energy density in the phonon gas.

C. Frequency- and wave-vector-dependent viscosity in phonon gas

To clarify the system described by the ET equations of Eqs. (1) and (2), we first consider one-branch phonon ET equation. We formally set the coupling constants to be zero, viz., $A=B=0$, in Eqs. (1) and (2), and the system reduces as the following:

$$\frac{\partial e}{\partial t} + c^2 \frac{\partial p_x}{\partial x} = 0$$

$$\frac{\partial p_x}{\partial t} + \frac{1}{3}\frac{\partial e}{\partial x} + \frac{\partial N_{\langle xx\rangle}}{\partial x} = -\frac{1}{\tau_{\mathrm{R}}} p_x,$$

$$\vdots$$

where we have dropped the mode suffix. Taking Fourier-Laplace transform, we obtain

$$\begin{bmatrix} s & ic^2q \\ i\frac{1}{3}q & s+\frac{1}{\tau_R}+\gamma_3(q,s) \end{bmatrix}\begin{bmatrix} e(q,s) \\ p(q,s) \end{bmatrix}=\begin{bmatrix} e(q,0) \\ p(q,0) \end{bmatrix}, \quad (8)$$

where s is the Laplace operator, and the contributions from the higher order moments than $p(q,s)$, namely, from $u_{\langle 2\rangle}, u_{\langle 3\rangle}, \ldots$, have been renormalized into $\gamma_3(q,s)$, which is regarded as a frequency- and wave-vector-dependent viscosity in a phonon gas.[6]

From Eq. (8), and taking into account the mutual independence between e and p, the correlation function $\langle e^*(q,0)e(q,s)\rangle$ is obtained as

$$\langle e^*(q,0)e(q,s)\rangle = \frac{1}{s+\dfrac{\frac{1}{3}c^2q^2}{s+\frac{1}{\tau_R}+\gamma_3(q,s)}}. \quad (9)$$

From Appendix A, it can be shown that the viscosity term, $\gamma_3(q,s)$, is defined by a recurrence relation as

$$\gamma_m(q,s)=\frac{\alpha_m c^2q^2}{s+\frac{1}{\tau}+\gamma_{m+1}(q,s)} \quad (m\geq 3),$$

and can be expressed as a continued-fraction form as

$$\gamma_3(q,s)=\cfrac{\alpha_3c^2q^2}{s+\frac{1}{\tau}+\cfrac{\alpha_4c_{(l)}^2q^2}{s+\frac{1}{\tau}+\cfrac{\alpha_5c_{(l)}^2q^2}{s+\frac{1}{\tau}+\cdots}}}, \quad (10)$$

where we have defined τ by

$$\frac{1}{\tau}\equiv\frac{1}{\tau_R}+\frac{1}{\tau_N}. \quad (11)$$

If we write the complex quantity $\gamma_3(q,s)|_{s=i\omega}$ as

$$\gamma_3(q,s)|_{s=i\omega}=\gamma_3'+i\gamma_3'', \quad (12)$$

where γ_3' and γ_3'' are real quantities, we obtain the scattering spectrum $S(q,\omega)$ as the real part of $\langle e^*(q,0)e(q,s)\rangle|_{s=i\omega}$

$$\begin{aligned} S(q,\omega)&=\mathrm{Re}[\langle e^*(q,0)e(q,s)\rangle|_{s=i\omega}] \\ &=\mathrm{Re}\left[\frac{\left(\frac{1}{\tau_R}+\gamma_3'\right)+i(\omega+\gamma_3'')}{(\omega_0^2-\omega^2-\gamma_3''\omega)+i\omega\left(\frac{1}{\tau_R}+\gamma_3'\right)}\right] \\ &=\frac{\omega_0^2\left(\frac{1}{\tau_R}+\gamma_3'\right)}{(\omega_0^2-\omega^2-\omega\gamma_3'')^2+\omega^2\left(\frac{1}{\tau_R}+\gamma_3'\right)^2}, \end{aligned} \quad (13)$$

where the natural frequency of the phonon gas has been introduced as

$$\omega_0\equiv\frac{1}{\sqrt{3}}cq. \quad (14)$$

If τ_R is sufficiently short such that $1/\tau_R \gg \gamma_3(q,t)$, then $\gamma_3(q,t)$ can be neglected and the right-hand side of Eq. (13) can be approximated as a Green function for a usual damped harmonic wave, whose resonance frequency and damping rate are given by $\sqrt{\omega_0^2-1/4\tau_R^2}$ and $1/\tau_R$, respectively. For weak damping, therefore, there can be a wave of phonon density, i.e., wavelike propagation of temperature, which is known as the "second sound.[1,2]" Thus, the equation set in Eqs. (1) and (2) can be viewed as two coupled second sounds, which are the temperature waves in the LA and TA phonon gases. Note that the macroscopic quantities such as "temperature" or "energy density" can be defined only if $1/\tau_R \gg \omega_0$, which ensures local thermal equilibrium within a time scale of $1/\omega_0$; such regime is referred to as "hydrodynamic" or "collision dominated." In contrast, if τ_R is long such that $\gamma_3(q,s)$ cannot be neglected, then, effects of frequency- and wave-vector-dependent viscosity appear as modifications to the resonance frequency and to the linewidth of the second sound as can be found in Eq. (13). In the latter case, local thermal equilibrium within a time scale of $1/\omega_0$ can no more be achieved, and this nonequilibrium regime is referred to as "ballistic" or "collisionless." These modifications to the second-sound frequency and linewidth can be thought as arising from memory effect in the dissipative processes in phonon gas,[6] and in that sense, $\gamma_3(q,s)$ is referred to as the "memory function." In the present case, if τ is short enough for $\gamma_4, \gamma_5, \ldots$ to be neglected, we see that $\gamma_3(q,\omega)$ describes a Debye-type relaxation. Since the inverse Laplace transform of $\gamma_3(q,s)$ yields that

$$\gamma_3(q,t)\approx\alpha_3c^2q^2e^{-t/\tau},$$

we see that the memory function can be approximated as an exponential function when $\gamma_4\tau \ll 1$. On the other hand, higher order terms must be incorporated if τ is long such that $\gamma_m\tau > 1$, and in general, an infinitely continued fraction must be considered as the memory function in the ballistic regime.

D. Coupling between two second sounds

In this section, we now consider the coupling between the two second sounds for the LA and TA phonon gases. From the discussions described in the Sec. II C, each of Eqs. (1) and (2) can be viewed as two damped harmonic waves (second sounds) with damping due to viscosity. The contributions to the viscosity from the moments of higher order than p can be renormalized into $\gamma_3(q,s)$ in the Fourier-Laplace space. Therefore, instead of considering the whole moment equations in Eqs. (1) and (2), we take only Eqs. (1a), (1b), (2a), and (2b), replacing $1/\tau_R^{(\lambda)}$ with $1/\tau_R^{(\lambda)}+\gamma_3^{(\lambda)}(q,s)$. Now the equation system in the Fourier-Laplace space becomes

$$\begin{bmatrix} s+2Ac_{(l)}^3 & ic_{(l)}^2 q & -2Ac_{(t)}^3 & 0 \\ i\frac{1}{3}q & s+[1/\tau_{\mathrm{R}}^{(l)}+\gamma_3^{(l)}(q,s)]+2Bc_{(l)}^5 & 0 & -2Bc_{(t)} \\ -Ac_{(l)}^3 & 0 & s+Ac_{(t)}^3 & ic_{(t)}^2 q \\ 0 & -Bc_{(l)}^5 & i\frac{1}{3}q & s+[1/\tau_{\mathrm{R}}^{(t)}+\gamma_3^{(t)}(q,s)]+Bc_{(t)}^5 \end{bmatrix} \begin{bmatrix} e^{(l)}(q,s) \\ p^{(l)}(q,s) \\ e^{(t)}(q,s) \\ p^{(t)}(q,s) \end{bmatrix} = \begin{bmatrix} e^{(l)}(q,0) \\ p^{(l)}(q,0) \\ e^{(t)}(q,0) \\ p^{(t)}(q,0) \end{bmatrix}. \quad (15)$$

By eliminating $p^{(l)}(q,s)$ and $p^{(t)}(q,s)$, we obtain two coupled wave equations for the second sounds for the LA and TA phonon gases

$$\begin{aligned} &\left\{ s^2 + \left[\frac{1}{\tau_{\mathrm{R}}^{(l)}} + \gamma_3^{(l)}(q,s) + 2c_{(l)}^3(A+Bc_{(l)}^2) \right] s + \frac{1}{3}c_{(l)}^2 q^2 \right. \\ &\quad \left. + 2Ac_{(l)}^3 \left[\frac{1}{\tau_{\mathrm{R}}^{(l)}} + \gamma_3^{(l)}(q,s) + Bc_{(l)}^2(2c_{(l)}^3 + c_{(t)}^3) \right] \right\} e^{(l)}(q,s) \\ &\quad - \left\{ 2c_{(t)}^3(A+Bc_{(l)}^2)s + 2Ac_{(t)}^3 \right. \\ &\quad \left. \times \left[\frac{1}{\tau_{\mathrm{R}}^{(l)}} + \gamma_3^{(l)}(q,s) + Bc_{(l)}^2(2c_{(l)}^3 + c_{(t)}^3) \right] \right\} e^{(t)}(q,s) \\ &= \left\{ s + \left[\frac{1}{\tau_{\mathrm{R}}^{(l)}} + \gamma_3^{(l)}(q,s) + 2c_{(l)}^3(A+Bc_{(l)}^2) \right] \right\} e^{(l)}(q,0) \\ &\quad - 2c_{(t)}^3(A+Bc_{(l)}^2)e^{(t)}(q,0) \end{aligned} \quad (16)$$

$$\begin{aligned} &\left\{ s^2 + \left[\frac{1}{\tau_{\mathrm{R}}^{(t)}} + \gamma_3^{(t)}(q,s) + c_{(t)}^3(A+Bc_{(t)}^2) \right] s + \frac{1}{3}c_{(t)}^2 q^2 \right. \\ &\quad \left. + Ac_{(t)}^3 \left[\frac{1}{\tau_{\mathrm{R}}^{(t)}} + \gamma_3^{(t)}(q,s) + Bc_{(t)}^2(2c_{(l)}^3 + c_{(t)}^3) \right] \right\} e^{(t)}(q,s) \\ &\quad - \left\{ c_{(l)}^3(A+Bc_{(t)}^2)s + Ac_{(l)}^3 \right. \\ &\quad \left. \times \left[\frac{1}{\tau_{\mathrm{R}}^{(t)}} + \gamma_3^{(t)}(q,s) + Bc_{(t)}^2(2c_{(l)}^3 + c_{(t)}^3) \right] \right\} e^{(l)}(q,s) \\ &= \left\{ s + \left[\frac{1}{\tau_{\mathrm{R}}^{(t)}} + \gamma_3^{(t)}(q,s) + c_{(t)}^3(A+Bc_{(t)}^2) \right] \right\} e^{(t)}(q,0) \\ &\quad - c_{(l)}^3(A+Bc_{(t)}^2)e^{(l)}(q,0), \end{aligned} \quad (17)$$

which can be expressed in a matrix form as

$$\begin{bmatrix} M_{11} & M_{12} \\ M_{21} & M_{22} \end{bmatrix} \begin{bmatrix} e^{(l)} \\ e^{(t)} \end{bmatrix} = \begin{bmatrix} m_{11} & m_{12} \\ m_{21} & m_{22} \end{bmatrix} \begin{bmatrix} e_0^{(l)} \\ e_0^{(t)} \end{bmatrix}. \quad (18)$$

Since the solution for Eqs. (16) and (17) is quite tedious, it is deferred to Appendix A. Although further simplifications are to be introduced below, the exact solution can still be obtained analytically, and its property is essentially the same as the solution with the simplification that is to be described below. As we expect for a coupled-oscillator system, the coupled second sounds described by Eqs. (16) and (17) can be diagonalized and the oscillations can be decomposed into two normal modes. The expressions for such normal modes become quite simple if we introduce an average group velocity and relaxation times for the LA and TA phonon gases

$$c_{(l)} = c_{(t)} = c, \quad \tau_{\mathrm{R}}^{(l)} = \tau_{\mathrm{R}}^{(t)} = \tau_{\mathrm{R}}, \quad \tau_{\mathrm{N}}^{(l)} = \tau_{\mathrm{N}}^{(t)} = \tau_{\mathrm{N}}. \quad (19)$$

First, the coupling constants A and B become, respectively, as

$$A = \frac{1}{3c^3}\left(\frac{1}{\tau_{\mathrm{R}}} + \frac{1}{\tau_{\mathrm{N}}} \right), \quad B = \frac{1}{3c^5 \tau_{\mathrm{N}}}. \quad (20)$$

If we assume a plane-wave solution, we find that the determinant of the characteristic matrix on the left-hand side of Eq. (18) for the system can be factorized into two simple quadratics in s

$$\begin{aligned} M_{11}M_{22} - M_{12}M_{21} &= \left\{ s^2 + \left[\frac{1}{\tau_{\mathrm{R}}} + \gamma_3(q,s) \right] s + \omega_0^2 \right\} \\ &\quad \times \left\{ s^2 + \left[\frac{2}{\tau} + \gamma_3(q,s) \right] s \right. \\ &\quad \left. + \left[\omega_0^2 + \frac{1}{\tau^2} + \frac{1}{\tau}\gamma_3(q,s) \right] \right\}. \end{aligned}$$

Setting $s \to i\omega$, we obtain the eigenvalues (the normal-mode frequencies) as

$$\omega_1 = \pm \sqrt{\omega_0^2 - \frac{1}{4}\left[\frac{1}{\tau_{\mathrm{R}}} + \gamma_3(q,s) \right]^2} + \frac{i}{2}\left[\frac{1}{\tau_{\mathrm{R}}} + \gamma_3(q,s) \right] \quad (21)$$

$$\omega_2 = \pm \sqrt{\omega_0^2 - \frac{1}{4}\gamma_3^2(q,s)} + i\left[\frac{1}{\tau} + \frac{1}{2}\gamma_3(q,s) \right]. \quad (22)$$

It is worth noting that, without the approximation made in Eq. (19), the determinant of the characteristic matrix is not to be factorized into such two simple quadratics in s; it is too complicated to display here. Even in that case, however, the four eigenvalues can be classified into two types qualitatively similar to Eqs. (21) and (22).

The eigenvector for $\omega = \omega_1$ is obtained as $e^{(l)}/2e^{(t)} = 1$, which indicates that the number densities of the phonons in the LA and TA phonon gases, i.e., the "component" temperatures, oscillate *in phase*. Since the "sum" of $e^{(l)}$ and $2e^{(t)}$ is the total energy density, e, which is proportional to the tem-

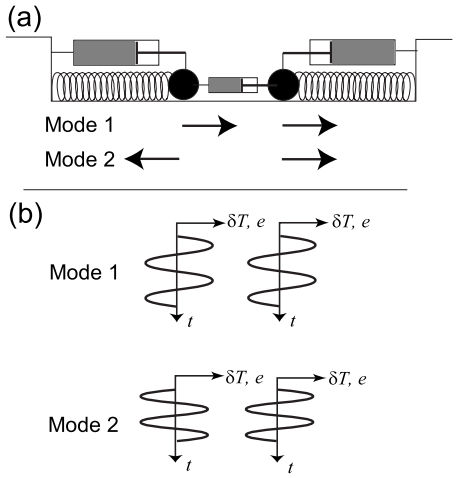

FIG. 1. Two coupled (a) mechanical oscillators and (b) second sounds (temperature waves). In both figures, Mode 1 and 2 are the "in-phase" and "out-of-phase" normal modes, respectively. In (b), δT and e represent the temperature fluctuation and the energy-density fluctuation, respectively. Note that the interaction between the two oscillators is much more effective in Mode 2 than in Mode 1.

perature change in the crystal, it is this "in-phase" mode that is directly detected as the temperature change in heat-pulse experiments.[20–24] If this mode is underdamped, the propagation of second sound is allowed, as it has been observed by several authors.[20–24] On the other hand, the eigenvector for $\omega=\omega_2$ is obtained as $e^{(l)}/2e^{(t)}=-1$, which indicates that the number densities of phonon in the LA and TA gases oscillate 180 *out of phase*. This "out-of-phase" mode is not observed as a wave (i.e., second sound) because Eq. (22) indicates that its damping is always faster than its frequency; this aspect will be proved in the later sections. It should be noted that, in experiments, only one second-sound mode can be observed although two second sounds are considered in the present model. This is because we cannot separately measure the component temperatures in the LA and TA phonon gases, but we can measure the "total" temperature, which corresponds to one of the two normal modes (i.e., the "in-phase" mode) formed by the two second-sound waves. Indeed, Dreyer and Struchtrup have shown[14] that two undamped second sounds[25] of speeds $c_{(l)}/\sqrt{3}$ and $c_{(t)}/\sqrt{3}$ give one second sound if the equation system is solved for the total energy density. The speed of such a second sound is given by[14]

$$V_{\mathrm{II}} = \sqrt{\frac{1}{3}\frac{\zeta_5}{\zeta_3}},$$

where $\zeta_n^{-1} \equiv \frac{1}{3}(1/c_{(l)}^n + 2/c_{(t)}^n)$. This velocity of second sound was also reported by Sussman and Thellung[26] and Beck and Beck.[27]

These two normal modes are similar to those in a mechanical two coupled oscillators,[28] which can be decomposed into the "in-phase" and "out-of-phase" modes, where the two weights move in the same and opposite directions, respectively [see Fig. 1(a)]. The "in-phase" mode does not affect the coupling spring (and/or dash pot) between the two weights if the two oscillators have the same mass and spring constant. In the "out-of-phase" mode, however, the length of the coupling spring (and/or dash pot) between the two weights changes significantly, resulting in the modification to the resonance frequency and/or to the damping rate. Without assuming Eq. (19), the two normal modes are not completely independent, but their properties are essentially similar to those mentioned above.

In the present system of "two coupled second sounds," the amplitudes of the two oscillations are the local temperatures in the LA and TA phonon gases [see Fig. 1(b)]. Therefore, if we assume the approximation as in Eq. (19), there is no dissipation from one temperature wave to the other in the "in-phase" mode (Mode1), because there is no temperature gradient between the two temperature waves; one of the two waves does not drag the other wave. Thus, in the "in-phase" normal mode, the viscous coupling between the second sounds for the LA and TA phonon gases is inactive when we assume the approximation as in Eq. (19), and is very weak even in general cases. On the other hand, in the "out-of-phase" normal-mode (Mode2), the local temperature changes in the two second sounds have opposite signs [see Fig. 1(b)], and hence, there is a temperature gradient between the two waves. Thus, one of the two waves strongly drags the other wave via the viscosity of the medium phonon gas.

If Eq. (19) is assumed, the spectra for the in-phase mode (Mode 1) and out-of-phase mode (Mode 2) are obtained, respectively, as

$$S_1(q,s) = \frac{1}{s + \dfrac{\frac{1}{3}c^2q^2}{s + \dfrac{1}{\tau_{\mathrm{R}}} + \gamma_3(q,s)}}, \tag{23}$$

and

$$S_2(q,s) = \frac{1}{s + \dfrac{1}{\tau} + \dfrac{\frac{1}{3}c^2q^2}{s + \dfrac{1}{\tau} + \gamma_3(q,s)}}. \tag{24}$$

$S_1(q,s)$ is identical with the right-hand side of Eq. (9), which is the spectrum for an independent (noninteracting) second sound: its properties have been described in Sec. II C. $S_2(q,s)$, on the other hand, includes the interaction between the two second-sound waves for the LA and TA phonon gases.

Since S_2 vanishes if there is no coupling between the two second sounds, S_2 can be interpreted as arising from energy and momentum dissipation from one second-sound mode to the other via the viscous coupling between the modes. Thus, the spectrum S_2 due to such a process may be interpreted as the "Mountain mode," which was first introduced by Mountain in the analysis of the light-scattering spectra in molecular fluids with internal degrees of freedom weakly coupled to the density fluctuations (sound wave) via frequency-dependent viscosity.[29] In our system, the second-sound

modes of LA and TA phonon gases are coupled, and one mode can behave as a dissipative counterpart for the other mode; they are just like the sound wave and the internal motions of molecules in a fluid. More detailed discussions are to be given in Sec. II G 4.

E. Phonon regime and Knudsen number

For systematic analyses, we set situations that are separated according to the magnitudes of the ratio of mean free path of phonons to the characteristic length scale. Such a ratio is referred to as the "Knudsen number" in the field of hydrodynamics. Since the characteristic length scale is the reciprocal of q (the magnitude of the wave-vector transfer) in scattering experiments, the Knudsen number in a phonon gas can be defined as

$$\mathrm{Kn} \equiv ql = qc\tau,$$

where l is the mean free path of phonons

$$l = c\tau.$$

In the phonon system we are concerned with, we have assumed two relaxation times, namely, τ_N and τ_R. Thus, we have to consider the phonon Knudsen numbers for both the normal and resistive processes, which we write as Kn_N and Kn_R

$$\mathrm{Kn}_N = qc\tau_N, \tag{25}$$

$$\mathrm{Kn}_R = qc\tau_R. \tag{26}$$

The overall Knudsen number is, then, given by

$$\mathrm{Kn} = (\mathrm{Kn}_R^{-1} + \mathrm{Kn}_N^{-1})^{-1} = qc\tau.$$

When $\mathrm{Kn}_N \ll 1$ or $\mathrm{Kn}_R \ll 1$, the situation is referred to as "hydrodynamic regime" because we can assume local thermal equilibrium within a length scale of q^{-1}. In the hydrodynamic regime, we can observe thermal diffusion, or thermal wave ("second sound"). When $\mathrm{Kn}_N \gg 1$ and $\mathrm{Kn}_R \gg 1$, the situation is referred to as "collisionless" or "ballistic" regime, where we cannot utilize macroscopic descriptions because macroscopic quantities such as temperature or entropy cannot be defined locally; in this case, we do not observe macroscopic phenomena such as diffusion or propagation of "temperature" or "entropy." Other general situations are categorized as "intermediate regime." Figure 2 shows how the phonon regimes are defined according to combinations of the phonon Knudsen numbers Kn_N and Kn_R.

In the hydrodynamic regime, i.e., when Kn is much smaller than unity, the ET-equation set in Eq. (1) reduce to a classical thermodynamic equation such as the heat diffusion equation or the heat wave equation for second sound. Such thermodynamic equations can be obtained even if we set γ_3 to be zero, which means that we neglect the moments higher than the momentum density. Therefore, the contributions of the higher order moments are considered to be silent if $\mathrm{Kn} \ll 1$. The higher order moments (or the viscosity term γ_3) begin to play significant roles when the nonequilibrium degree is increased such that $\mathrm{Kn} \gtrsim 1$.

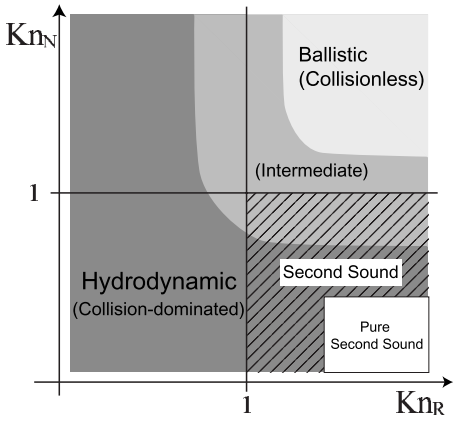

FIG. 2. Phonon regimes and phonon Knudsen numbers. Kn_R and Kn_N are defined in Eqs. (25) and (26), respectively. The hatched region corresponds to the "second-sound regime," where a wavelike propagation of heat is expected to exist in solids.

F. Asymptotic expression for the spectrum

The continued-fraction expansion is advantageous in that we can approximate the spectrum with asymptotic forms of the component fractions in Eq. (10), viz., $\lim_{n\to\infty} \gamma_n(q,s)$, assuming equal relaxation times for a mode.[6] In that case, one has only to provide a continued fraction to a certain order ($n \sim 30$ has been turned out to be sufficient), then to terminate it with an asymptotic form obtained from the relation[6]

$$\gamma_\infty(q,s) = \frac{1}{(s+1/\tau) + \alpha_\infty c^2 q^2 \gamma_\infty(q,s)},$$

which gives

$$\gamma_\infty(q,s) = \frac{2}{c^2 q^2}[-(s+1/\tau) + \sqrt{(s+1/\tau)^2 + c^2 q^2}], \tag{27}$$

where we note that $\alpha_\infty = \lim_{n\to\infty} \alpha_n = 1/4$. By terminating the continued fractions in Eq. (10) with the asymptotic form at sufficiently deep level, namely, at $n_{\max} = 31$,[5,14] where $n_{\max}$ is the highest order of moment, Eqs. (23) and (24) can be applied *continuously* from thermal equilibrium even to far nonequilibrium regime because $\gamma_3(q,s)$ so terminated includes effectively infinite orders of moments.

For $S_2(q,s)$, we can express the right-hand side of Eq. (24) in a more compact form if we infinitely expand the continued fraction in $\gamma_3(q,s)$ (see Appendix B)

$$\mathrm{Im}[S_2(q,s)|_{s=i\omega}] = \frac{1}{2cq}\{\ln[(\omega+cq)^2\tau^2+1] - \ln[(\omega-cq)^2\tau^2+1]\}, \tag{28}$$

$$\mathrm{Re}[S_2(q,s)|_{s=i\omega}] = \frac{1}{2cq}[\tan^{-1}(\omega+cq)\tau - \tan^{-1}(\omega-cq)\tau]. \tag{29}$$

The scattering spectrum is given from Eq. (29); the right-hand side is a difference of two arctangent functions. The right-hand side of Eq. (28) is a difference of two logarithmic

functions, and Eqs. (28) and (29) are related by the Kramers-Kronig relation. Since the expressions in Eqs. (28) and (29) contain the infinite hierarchy of the frequency- and wave-vector-dependent viscosity, we may use Eqs. (28) and (29) as a response function of Mode 2 for any combination of $\mathrm{Kn_N}$ and $\mathrm{Kn_R}$.

The spectral function of the lowest order with the asymptotic expressions of Eq. (27) corresponds to that in the case that $n_{\max}=2$ and $\gamma_3(q,s)=\gamma_\infty(q,s)=2[\sqrt{c^2q^2+(s+1/\tau)^2}-(s+1/\tau)]$. In that case, $\gamma_3'(q,\omega)$ and $\gamma_3''(q,\omega)$ in Eq. (12) are given, respectively, by

$$\gamma_3'(q,\omega)=\frac{8}{15}\left(z'-\frac{1}{\tau}\right),\quad \gamma_3''(q,\omega)=\frac{8}{15}(z''-\omega), \tag{30}$$

where z' and z'' are defined as in $z=\sqrt{c^2q^2+(i\omega+1/\tau)^2}=z'+iz''$, with

$$z'=\mathrm{Re}[\sqrt{c^2q^2+(i\omega+1/\tau)^2}]=\frac{1}{\sqrt{2}}\sqrt{\sqrt{\left(c^2q^2-\omega^2+\frac{1}{\tau^2}\right)^2+\frac{4\omega^2}{\tau^2}}+\left(c^2q^2-\omega^2+\frac{1}{\tau^2}\right)},$$

$$z''=\mathrm{Im}[\sqrt{c^2q^2+(i\omega+1/\tau)^2}]$$
$$=\mathrm{sign}(\omega)\times\frac{1}{\sqrt{2}}\sqrt{\sqrt{\left(c^2q^2-\omega^2+\frac{1}{\tau^2}\right)^2+\frac{4\omega^2}{\tau^2}}-\left(c^2q^2-\omega^2+\frac{1}{\tau^2}\right)}.$$

If we expand the continued fraction $\gamma_3(q,s)$ further, i.e., if $n_{\max}=3$ and $\gamma_4(q,s)=\gamma_\infty(q,s)$, then γ_3' and γ_3'' are given as follows:

$$\gamma_3'(q,\omega)=\frac{4}{15}c^2q^2\times\frac{35}{17}\frac{1/\tau+\frac{18}{17}z'}{\left(\omega+\frac{18}{17}z''\right)^2+\left(1/\tau+\frac{18}{17}z'\right)^2}, \tag{31}$$

$$\gamma_3''(q,\omega)=-\frac{4}{15}c^2q^2\times\frac{35}{17}\frac{\omega+\frac{18}{17}z''}{\left(\omega+\frac{18}{17}z''\right)^2+\left(1/\tau+\frac{18}{17}z'\right)^2}. \tag{32}$$

Note that $\gamma_3(q,\omega)$ as given above can be approximated as a Debye-type relaxational mode (a central Lorentzian) if hydrodynamic regime ($cq\tau\ll 1$) is assumed

$$\gamma_3(q,\omega)\approx\frac{\tau}{1+i\omega\tau}\quad(n_{\max}=3,\gamma_4=\gamma_\infty).$$

G. Hydrodynamic regime

1. Second sound

If $\mathrm{Kn_R}\ll 1$ or $\mathrm{Kn_N}\ll 1$, one can show from Eq. (30) that, for $n_{\max}=2$ and $\gamma_3=\gamma_\infty$,[30]

$$\gamma_3'(q,\omega)\to\frac{4}{15}c^2q^2\tau,\quad\text{and}\quad\gamma_3''(q,\omega)\to 0,$$

which give

$$S_1(q,\omega)\approx\frac{2\omega_0^2\Gamma_{ss}}{(\omega^2-\omega_0^2)^2+4\omega^2\Gamma_{ss}^2}, \tag{33}$$

where we have defined

$$\Gamma_{ss}\equiv\frac{2}{5}\omega_0^2\tau_N+\frac{1}{2\tau_R}=\frac{2}{15}c^2q^2\tau_N+\frac{1}{2\tau_R}. \tag{34}$$

$S_1(q,\omega)$ in Eq. (33) is the spectrum for a damped harmonic oscillator (DHO), and is essentially identical with that obtained earlier by other authors[10,18,31,32] except the differences in the numerical factors in Γ_{ss}. ω_0 defined in Eq. (14) is the natural frequency of the phonon gas, and it corresponds to the frequency of an undamped "thermal wave." Γ_{ss} defined in Eq. (34) is the damping rate of the thermal wave. Note that Γ_{ss} depends not only on τ_R but also on τ_N, c, and q, and it has opposite dependences on τ_N and on τ_R, i.e., the shorter τ_N (τ_R) gives the smaller (larger) Γ_{ss}.

If $\Gamma_{ss}<\omega_0$ holds, the thermal wave is underdamped and a resonance occurs at a frequency

$$\omega_{ss}=\sqrt{\omega_0^2-\Gamma_{ss}^2} \tag{35}$$

$$\approx\omega_0\left(1-\frac{2}{5}\frac{\tau_N}{\tau_R}\right), \tag{36}$$

which is the frequency of "second sound," and this resonance effect is referred to as the "second-sound resonance." Rather than the familiar diffusive transport of heat energy, the second sound is a wavelike propagation of heat at a finite propa-

gation speed $v_{ss} \approx c/\sqrt{3}$, In order to have such an *equilibrated* thermal wave as a well-defined collective excitation of phonons, we need, not only the weak-damping condition $\Gamma_{ss} \ll \omega_0$, but also the hydrodynamic regime, i.e., $\mathrm{Kn}_N \ll 1$ or $\mathrm{Kn}_R \ll 1$ because there must be sufficient number of thermal phonons within the relevant scales of space and time. The simultaneous requirements can be expressed in an inequality as

$$\Gamma_{ss} \ll \omega_0 \ll \tau_N^{-1}.$$

From Eq. (34), this can be alternatively expressed in a well-known[10] form as

$$\tau_R^{-1} \ll \omega_0 \ll \tau_N^{-1},$$

which is called the "window condition" for propagation of second sound in solids. The window condition can be expressed also as

$$\mathrm{Kn}_N \ll 1 \ll \mathrm{Kn}_R, \tag{37}$$

which is clearly stating that one simultaneously requires frequent *N* processes and infrequent *R* processes within a length scale of q^{-1}. In Fig. 2, the region labeled as "pure second sound" corresponds to the condition of Eq. (37). In this regime, "pure" second sound is expected, and its spectrum should be a very sharp doublet located at $\omega_{ss} \approx \pm cq/\sqrt{3}$.

2. Thermal diffusion

If $\Gamma_{ss} > \omega_0$, then the second sound is overdamped and cannot propagate. This is the thermal diffusion effect, which is a much more common phenomenon in thermal transport in most materials. In this case, $S_1(q,\omega)$ is reduced approximately to a central peak

$$S_1(q,\omega) \approx \frac{\Gamma_{th}}{\omega^2 + \Gamma_{th}^2}, \tag{38}$$

which is the well-known "thermal Rayleigh component"[17] with a width proportional to q^2 as

$$\Gamma_{th} = D_{th} q^2. \tag{39}$$

D_{th} is the thermal diffusivity in a well-known kinetic expression as

$$D_{th} = \frac{1}{3} c^2 \tau_R. \tag{40}$$

The width can be alternatively expressed as

$$\Gamma_{th} = \omega_0^2 \tau_R.$$

3. Properties of $S_2(q,\omega)$ and total spectrum

Setting $cq\tau \ll 1$ in the right-hand side of Eq. (29), we see that

$$S_2(q,\omega) \approx \frac{1}{2cq} \times 2cq\tau \frac{\partial}{\partial(\omega\tau)} \tan^{-1} \omega\tau = \frac{\Gamma_2}{\omega^2 + \Gamma_2^2}, \tag{41}$$

where

$$\Gamma_2 = \frac{1}{\tau} = \frac{1}{\tau_N} + \frac{1}{\tau_R}.$$

Thus, the linewidth of $S_2(q,\omega)$ corresponds to the mean frequency of the collisions between the phonons. Since τ is an averaged relaxation time over the whole thermal phonons in the Brillouin zone, τ is considered to have no dependence on frequency and wave vector of thermal phonons.[14] Thus, τ should be independent of q. The width Γ_2 is much broader than ω_0 and than Γ_{th} because we are assuming the hydrodynamic regime ($cq\tau_N \ll 1$ or $cq\tau_R \ll 1$). Thus, the thermal-DHO spectrum, $S_1(q,\omega)$, should be superposed on this much broader unshifted Lorentzian of $S_2(q,\omega)$ as

$$S_{total}(q,\omega) = P_1 \frac{2\omega_0^2 \Gamma_{ss}}{(\omega^2 - \omega_0^2)^2 + 4\omega^2 \Gamma_{ss}^2} + P_2 \frac{\Gamma_2}{\omega^2 + \Gamma_2^2}, \tag{42}$$

where P_1 and P_2 are the weighting coefficients for $S_1(q,\omega)$ and $S_2(q,\omega)$, respectively.

In thermal diffusion regime, the resistive process is dominant, and Γ_2 is effectively equal to $1/\tau_R$. Thus, we have a useful relation between Γ_{th} and Γ_2 as

$$\Gamma_{th}\Gamma_2 \approx \frac{1}{3} c^2 q^2 = \omega_0^2, \tag{43}$$

i.e., the product of the linewidths of thermal Rayleigh and Mountain modes is almost temperature independent at high temperatures. Equation (43) also states that

$$\sqrt{\gamma_1 \gamma_2} = \frac{1}{\sqrt{3}}, \tag{44}$$

where $\gamma_1 = \Gamma_{th}/cq$ and $\gamma_2 = \Gamma_2/cq$ are the linewidths normalized by the average Brillouin shift.

4. Interpretation of the spectral components in the hydrodynamic regime

It is important to note that the thermal relaxation (thermal diffusion) and the fast relaxation (collisions between phonons) should never be discussed separately. Rather, we see that the two spectra, $S_1(q,\omega)$ and $S_2(q,\omega)$, reflect two limiting aspects in a medium: the slow relaxation corresponds to the fluctuations just in the vicinity of local thermal equilibrium, whereas the fast one to the kinetic processes, i.e., the collisions, which are the nonequilibrium processes essential for thermal equilibrium to be locally established. Therefore, we see the "duality" of a phonon gas; we see both equilibrium and nonequilibrium processes simultaneously in Eq. (42). It should also be emphasized that such a spectral structure of the dual fluctuation can be observed only if the characteristic length (or time) scale in the scattering experiment lies between the two length scales for thermal diffusion and interparticle collision, i.e., a relation,

$$l \ll q^{-1} \ll c/(D_{th} q^2) \tag{45}$$

is required for the two spectra to be clearly resolved. Therefore, the selection of a length scale q^{-1} is critical in studying

the nonequilibrium phonon dynamics in crystals, and we see that light-scattering experiments can offer a good value since $10 \lesssim q^{-1} \lesssim 100$ nm. Note that the mean free path of phonons can range from ~ 1 to ~ 1000 nm according to the temperature, indicating that temperature change can break the inequality [Eq. (45)]. Since an average Brillouin frequency $\bar{\omega}_B = qc$ can be regarded as a characteristic frequency in light scattering in a phonon gas,[7] Eq. (45) can be written in the frequency domain as

$$D_{\text{th}} q^2 \ll \bar{\omega}_B \ll \bar{\tau}^{-1},$$

which states that the Brillouin line should appear in the middle frequency range between the two central peaks of S_1 and S_2.

Similar discussions should be able to apply to any scattering experiments for any gas model. In such general cases, D_{th} should be replaced with a generalized diffusivity for constituent particles or excitations. In fact, superionic conductors exhibited similar double quasielastic spectrum in light-[33] and neutron-[34] scattering experiments and the narrow and broad linewidths were tentatively attributed to the ion diffusion rate and the mean hopping rate of the conducting ions, respectively. This is very similar in nature to the present case as was hinted long ago.[35]

H. Ballistic regime (collisionless regime)

If both N and R processes become infrequent such that $\text{Kn}_N, \text{Kn}_R \gtrsim 1$, the approximate expression of Eq. (42) in the hydrodynamic regime is not valid, and effects of higher order moments set in. If we retain the approximation defined in Eq. (19), S_1 and S_2 are given, respectively, from Eqs. (13) and (29) as

$$S_1(q,\omega) = \frac{\omega_0^2 \left(\frac{1}{\tau_R} + \gamma_3' \right)}{(\omega_0^2 - \omega^2 - \omega \gamma_3'')^2 + \omega^2 \left(\frac{1}{\tau_R} + \gamma_3' \right)^2},$$

$$S_2(q,\omega) = \frac{1}{2cq} [\tan^{-1}(\omega + cq)\tau - \tan^{-1}(\omega - cq)\tau],$$

where $\gamma_3'(q,\omega)$ and $\gamma_3''(q,\omega)$ are the real and imaginary parts of $\gamma_3(q,s)|_{s=i\omega}$ defined in Eq. (10), respectively. As the ballistic regime is approached, the widths of S_1 and S_2 approach each other as shown in Fig. 3, where the Normal process of phonon collision is ignored by setting $\tau_N \gg \tau_R$. For small values of τ_R, the spectra of S_1 and S_2 correspond to the thermal-diffusion mode and the Mountain mode, respectively, and both spectra are well approximated as Lorentzians, as we have described in Sec. II G. As τ_R becomes longer, the narrow quasielastic component, S_1, broadens whereas the broad component S_2 narrows. However, the two widths of S_1 and S_2 converges to cq, which is the averaged Brillouin frequency $\bar{\omega}_B$. In fact, in the extreme limit of the ballistic regime, we can set $\tau \to \infty$, and we see, from Eqs. (23) and (24) that $S_1(q,\omega)$ and $S_2(q,\omega)$ coincide with each other

$$S_1(q,\omega) = S_2(q,\omega) = \frac{\omega_0^2 \gamma_3'(q,\omega)}{[\omega_0^2 - \omega^2 - \gamma_3''(q,\omega)\omega]^2 + \omega^2 \gamma_3'^2(q,\omega)}. \tag{46}$$

The convergence of S_1 and S_2 is shown in Fig. 3 for $\text{Kn}_R = 100$ although the line shape of S_1 is slightly distorted due to a crude approximation, in which we set $\gamma_4 \to \gamma_\infty$ in tracing the spectra of S_1.

The rectangular line shape in the ballistic limit can be checked qualitatively as the following. If we replace the continued fraction $\gamma_3(q,s)$ with $\gamma_\infty(q,s)$ in Eq. (30), we get

$$\gamma_3'(q,\omega) \to \frac{8}{15} cq \sqrt{c^2 q^2 - \omega^2}, \quad \gamma_3''(q,\omega) \to -\frac{8}{15}\omega.$$

Substituting the above expressions of $\gamma_3'(q,\omega)$ and $\gamma_3''(q,\omega)$ into the right-hand side of Eq. (46) yields a spectrum of the form

$$S_1(q,\omega) = S_2(q,\omega) = \frac{24\omega_0^2 \sqrt{c^2 q^2 - \omega^2}}{-\omega^4 - \frac{6}{5}\omega_0^2 \omega^2 + 15\omega_0^4} \quad (|\omega| \le cq). \tag{47}$$

The numerator and denominator of the right-hand side of Eq. (47) are an ellipse and a convex quartic curve, respectively. Since the latter is close to an ellipse in shape, the spectral shape is almost flat for $-cq \le \omega \le cq$, and it has vertical walls at $\omega = \pm cq$.

If we do not employ the asymptotic form $\gamma_\infty(q,s)$ and cut the continued fraction at $n = n_{\max}$, i.e., if we set $\gamma_{n_{\max}+1} = 0$, the spectrum in the highly ballistic regime exhibits $n_{\max}$ sharp peaks[5,36] as we show in Fig. 4, where $n_{\max}$ and Kn_R are varied ($\text{Kn}_N \to \infty$ is assumed for simplicity). In general, it can be shown that these peaks are located at $\omega(i) = cq \cos \phi_{n_{\max}}(i)$, and their heights are $h(i) \propto \sin \phi_{n_{\max}}(i)$, where $\phi_{n_{\max}}(i) = i\pi/(n_{\max}+1)$, and i is an integer (for detailed discussions, see Appendix B). The spectral formula in the ballistic limit is, then, given in the form

$$S_{\text{bal}}(\omega, q,) \propto \sum_{i=1}^{n_{\max}} \sin \phi_{n_{\max}}(i) \frac{1/\tau^2}{[\omega - cq \cos \phi_{n_{\max}}(i)]^2 + 1/\tau^2}, \tag{48}$$

where Lorentzian line shape is introduced, and a common linewidth, $1/\tau$, has been introduced for all the peaks. The behavior of the spectra in the ballistic limit, i.e., $\text{Kn}_R = 1000$ shown in Fig. 4 can be fully reproduced by Eq. (48).

The comblike peak distribution seen in Fig. 4 is apparently due to the lack of number of moments. In fact, in Fig. 4, the spectrum for $n_{\max} = 30$ and $\text{Kn}_R = 100$ is comblike whereas that for $n_{\max} = 300$ and $\text{Kn}_R = 100$ is rectangular in shape. To include infinite number of higher order moments, we only have to replace the summation in Eq. (48) with an integral, and we obtain the spectrum with infinite number of moments ($n_{\max} \to \infty$)

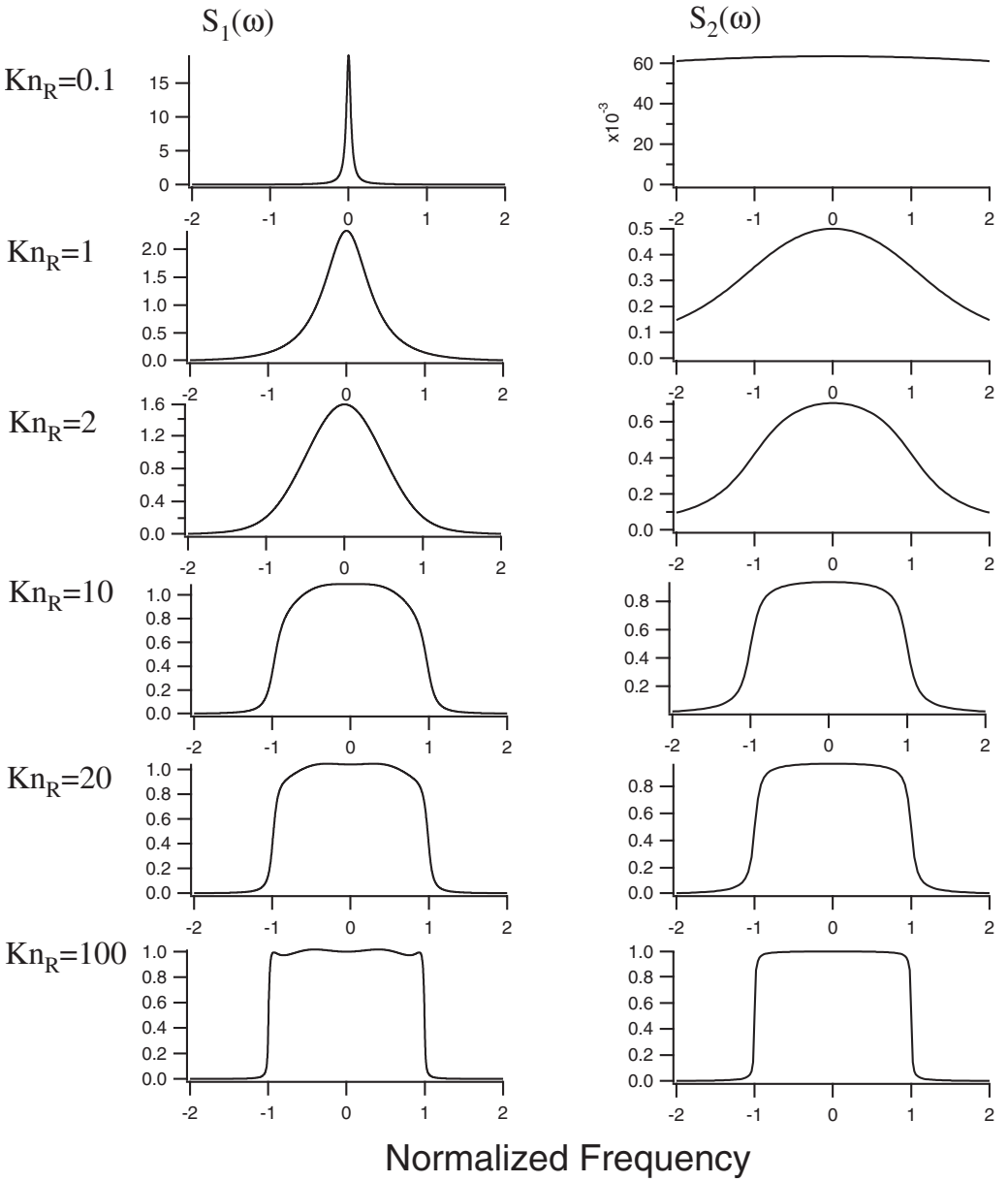

FIG. 3. $\mathrm{Kn_R}$ dependence of the spectra of S_1 and S_2. The vertical axes are scaled in arbitrary units. The horizontal axes are measured in units of cq, which is the averaged Brillouin frequency.

$$S_{\mathrm{bal}}(\omega,q) \propto \int_0^{\pi} \sin\phi \frac{1/\tau^2}{(\omega - cq\cos\phi)^2 + 1/\tau^2} d\phi. \quad (49)$$

The right-hand side can be analytically integrated to give

$$S_{\mathrm{bal}}(\omega,q) \propto \tan^{-1}(\omega + cq)\tau - \tan^{-1}(\omega - cq)\tau, \quad (50)$$

which is identical with the right-hand side of Eq. (29). Setting $\tau \to \infty$ in Eq. (50), we actually obtain a rectangular function

$$\lim_{\tau\to\infty} S_{\mathrm{bal}}(q,\omega) = \begin{cases} 1 & (|\omega| < cq) \\ \frac{1}{2} & (\omega = \pm cq) \\ 0 & (|\omega| > cq) \end{cases} = \mathrm{rect}\left(\frac{\omega}{2cq}\right).$$

The light scattering in the ballistic regime can be viewed also as arising from elastic scattering from individual phonons traveling in all directions. Similar effect is observed in rarefied gasses, in which the individual molecules elastically scatter the incident radiation as "moving mirrors" with the velocity components following the Maxwell-Boltzmann velocity distribution, giving rise to a Doppler-broadened elastic spectrum, i.e., a central Gaussian spectrum.[5,37] In general, the spectrum obtained from individual scatterers in the low-density limit is given by[5]

$$S(q,\omega) \propto \mathrm{Re}\left[\int \frac{\tilde{f}(\boldsymbol{c})}{s - i\boldsymbol{c}\cdot\boldsymbol{q} + 1/\tau} d\boldsymbol{c}\right]_{s=i\omega},$$

where $\tilde{f}(\boldsymbol{c})$ is the velocity distribution for the scatterers; for ideal (massive) gasses $\tilde{f}(\boldsymbol{c}) \propto e^{-mc^2/2k_BT}$ (Maxwell-Boltzmann

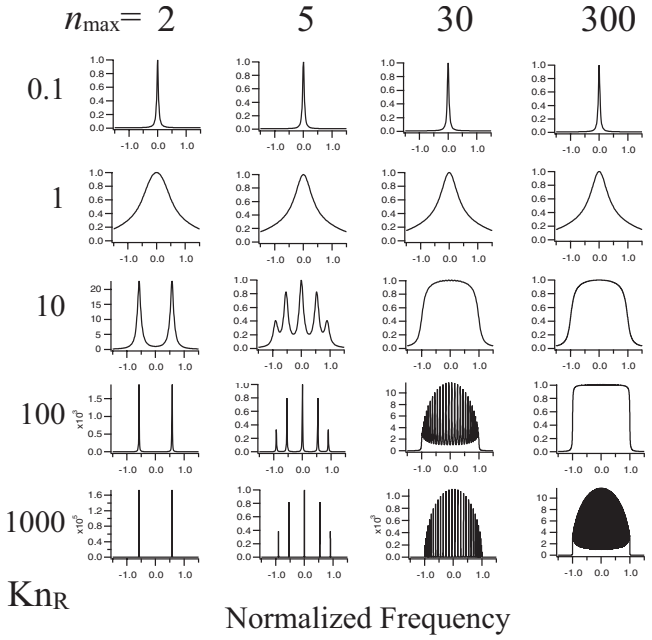

FIG. 4. Spectrum in the ballistic limit without the asymptotic termination. For $Kn_R=0.1$, there is only one peak (central peak) due to thermal diffusion. For larger values of Kn_R, splittings of the spectra are seen.

distribution), and for an *isotropic* phonon gas

$$\tilde{f}(\boldsymbol{c}) = \frac{1}{2}\sin\phi, \quad \left(\phi = \cos^{-1}\frac{\boldsymbol{c}\cdot\boldsymbol{q}}{cq}\right).$$

Thus, the scattering spectrum from individual phonons in an isotropic phonon gas is given as

$$S(q,\omega) \propto \mathrm{Re}\left[\int_0^\pi \frac{\sin\phi}{s - iqc\cos\phi + 1/\tau} d\phi\right]_{s=i\omega}$$
$$= \tan^{-1}(\omega + cq)\tau - \tan^{-1}(\omega - cq)\tau,$$

which is identical with Eq. (50), and it becomes flat $(-cq \le \omega \le cq)$ as $\tau \to \infty$.

If elastic anisotropy of a crystal is taken into account, then the limiting spectrum can exhibit some structure as reported by Farhi *et al.*[38,39] in their analysis based on two-phonon difference light scattering in $KTaO_3$. They found that doubletlike spectrum can appear if $\boldsymbol{q}$ is in a direction where there is local minimum for the sound velocity.

I. Two-phonon difference light scattering

It must be pointed out that Eqs. (48)–(50) can also be viewed as a light-scattering spectrum from pairs of phonons on a same phonon-dispersion branch: these phonons are simultaneously created and annihilated.[18,38–42] Such a scattering mechanism is referred to as two-phonon difference scattering (TPDS). The TPDS is a consequence of the second-order Raman effect, in which a pair of elementary excitations participates;[37] this effect arises from the second term in the right-hand side of Eq. (7).

The TPDS is the lowest order approximation for describing the interaction of photon (light) with phonons (*not* with a *single* phonon as in the first-order Raman scattering). In the TPDS, one of the two phonons is created while the other is simultaneously annihilated: the energy and momentum conservation is fulfilled among the two participating phonons and light. Let the incident light have a frequency and wave vector as $(\omega_{inc}, \boldsymbol{k}_{inc})$, and the scattered light $(\omega_{scat}, \boldsymbol{k}_{scat})$. The energy and momentum conservation in a two-phonon difference process is expressed as

$$\omega = \omega_{scat} - \omega_{inc} = \omega_i(\boldsymbol{k}_2) - \omega_j(\boldsymbol{k}_1),$$
$$\boldsymbol{q} = \boldsymbol{k}_{scat} - \boldsymbol{k}_{inc} = \boldsymbol{k}_2 - \boldsymbol{k}_1, \tag{51}$$

where $\omega_i(k)$ is the frequency of a phonon in mode i, and $\boldsymbol{k}_1$ and $\boldsymbol{k}_2$ are the wave vectors of the relevant phonons. Note that $q \ll k_1, k_2$ and that $\omega \ll \omega_1, \omega_2$ in light-scattering experiments. The TPDS from different phonon modes, i.e, the case in which $i \neq j$, requires that two different phonon modes be degenerated at points in the Brillouin zone. Since such points are usually located at the zone boundaries, it is not expected that TPDS from different phonon modes is dominant at low temperatures. Hence, in the ballistic regime, where there are few phonons excited, the phonons participating in the TPDS should belong to the same branch, viz., $i=j$. Thus, the TPDS should be "intramode" in the ballistic regime.[43]

Assuming an isotropic phonon dispersion, and letting the angle between $\boldsymbol{q}$ and $\boldsymbol{k}_2$ be φ, a single TPDS yields[42] a frequency shift of $\omega(\varphi) = cq\cos\varphi$. If the two phonons have lifetimes, the spectrum from a single-scattering process may be regarded as a Lorentzian with a "pair width"[44] of $1/\tau$.[38] Thus, summing up all the contributions from the phonon pairs in the Brillouin zone, we have[45]

$$S_{TPDS}(\omega,q) \propto \int_0^\pi \sin\varphi \frac{1/\tau^2}{(\omega - cq\cos\varphi)^2 + 1/\tau^2} d\varphi$$
$$= \tan^{-1}(\omega + cq)\tau - \tan^{-1}(\omega - cq)\tau. \tag{52}$$

This is identical with the spectrum in the ballistic limit presented in Eqs. (49) and (50) if we identify φ with ϕ. Therefore, the comblike spectrum in the ballistic limit in Fig. 4 may be viewed also as a collection of scattering spectra due to two-phonon difference processes. The form of TPDS as in Eq. (52) was also reported in Ref. 39 with more rigorous discussions.

Although we assumed the ballistic regime so far, let us investigate the spectrum of Eq. (52) in the hydrodynamic regime. As we have shown in Eq. (41), the differential arctangent spectrum as in the right-hand side of Eq. (52) can be approximated as a Lorentzian with a width of $\Gamma_2 = \tau^{-1}$. Since two-phonon approximation is not possible in the hydrodynamic regime in a strict sense, we must consider that higher order interactions between the participating phonon pairs are effectively renormalized in the pair width. Such renormalization may be characterized as a ladder-type diagram for the self-energy in the Green function technique,[18,19,32,46] in which "first sound," "second sound (including thermal diffusion)," and "nonthermodynamic dielectric fluctuations" have been introduced. Among such contributions in the self-energy, the present TPDS corresponds to the "nonequilib-

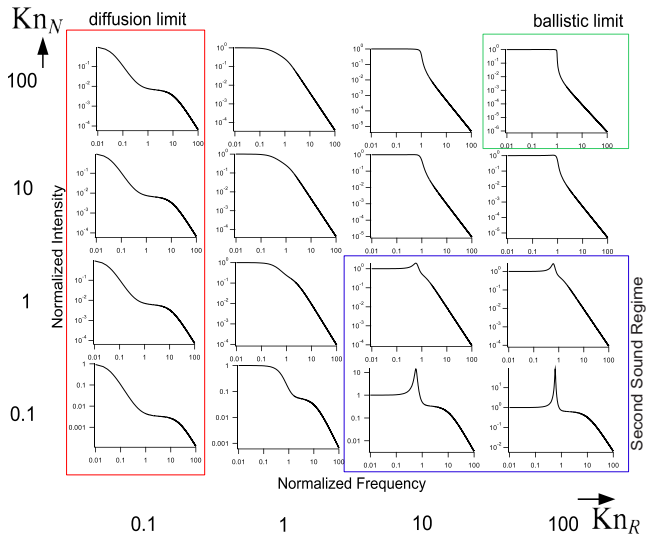

FIG. 5. (Color online) A chart of light-scattering spectra from a phonon gas for combinations of $(\mathrm{Kn_R}, \mathrm{Kn_N})$. All the spectra are plotted on log-log scales. We set $n_{\max}=5$ and $\gamma_6=\gamma_\infty$ in calculating these spectra.

rium" contribution, which can alternatively be interpreted as the "Mountain mode" in crystals in Klein's terminology.[19]

Summarizing this section, we have seen that S_{TPDS} is always coincides with S_2 regardless of the phonon regime. Therefore, S_2 may be regarded as arising from light scattering from two-phonon difference processes on the same phonon dispersion, and we may always write $S_2(q,\omega)$ as

$$S_2(q,\omega)=\frac{1}{2\pi cq}[\tan^{-1}(\omega+cq)\tau-\tan^{-1}(\omega-cq)\tau], \tag{53}$$

where a normalizing factor has been introduced such that the integrated intensity is equal to 1. $S_2(q,\omega)$ in this "differential arctangent" form can cover spectrum shapes continuously from the broad central Lorentzian in the hydrodynamic regime to the rectangular spectrum in the ballistic regime.

J. Summary of spectral variation

To summarize theory section, we present, in Fig. 5, a chart of the light-scattering spectra calculated for a phonon gas, covering possible major combinations of $(\mathrm{Kn_R}, \mathrm{Kn_N})$. Here, we still retain the approximation as in Eq. (19) for simplicity. Even without the approximation, the properties of the calculated spectra are essentially the same except that each linewidth of S_1 and S_2 slightly differs from that in the approximated case. We have set $n_{\max}=5$ and $\gamma_6(q,s)=\gamma_\infty(q,s)$, which turned out to be sufficient for the present demonstration. Note that all the graphs are on doubly logarithmic scales. Figure 2 may be helpful to check the correspondence between the phonon regimes and the phonon Knudsen numbers.

In the hydrodynamic regime ($\mathrm{Kn_N}\ll 1$ or $\mathrm{Kn_R}\ll 1$), there is always a broad quasielastic component at the bottom of the spectral structure: this component is $S_2(q,\omega)$. On the top

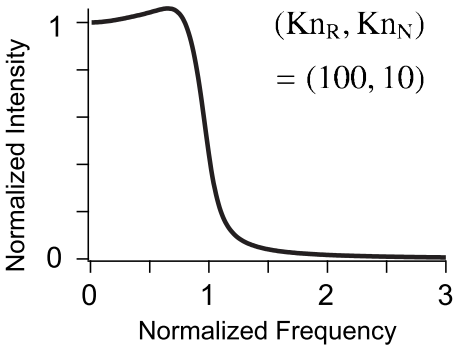

FIG. 6. Shifted-peak structure in the collisionless regime $(\mathrm{Kn_R}, \mathrm{Kn_N})=(100, 10)$. Both axes are on linear scales.

of S_2 spectra, there are either narrower quasielastic component due to thermal diffusion or inelastic peaks due to second-sound resonance; both of these are S_1's. The coexistence of S_1 and S_2 indicates the duality of a relaxation processes in a phonon gas. The origin of S_2 can be interpreted as the followings (1) the nonequilibrium counterpart of fluctuations (relaxation processes) in a phonon gas, (2) the Mountain mode due to frequency-dependent viscosity in a crystal, or (3) two-phonon difference light scattering on the same phonon dispersion, each of which statements is physically equivalent to one another.

The left column of the Fig. 5 corresponds to the diffusion limit, for which $\mathrm{Kn_R}\ll 1$, i.e., the R process is dominant, and the spectrum consists of two unshifted Lorentzians. The linewidths for the narrow and broad quasielastic components are $\Gamma_1=D_{\mathrm{th}}q^2=\frac{1}{3}c^2q^2\tau_{\mathrm{R}}$ and $\Gamma_2=\tau^{-1}=\tau_{\mathrm{R}}^{-1}+\tau_{\mathrm{N}}^{-1}$, respectively.

The lower right regions in Fig. 5, i.e., $(\mathrm{Kn_R}, \mathrm{Kn_N})=(100, 0.1)$, corresponds to the "pure" second-sound regime because of Eq. (37), and a very sharp peak due to second-sound resonance is found. However, it should be pointed out that the resonance peaks due to second sound are found in a wider range in Fig. 5, viz., $\mathrm{Kn_N}\lesssim 1\lesssim \mathrm{Kn_R}$. This means that the window condition for the observation of the second-sound peak in light-scattering experiments may be rather tolerant.

The upper right region in Fig. 5, i.e., the region $\mathrm{Kn_R}, \mathrm{Kn_N}\gg 1$, corresponds to the ballistic limit. As the ballistic limit is approached, S_1 and S_2 approach each other, and in the limit of $\tau\to\infty$, both spectra converge into a rectangular shape with a cut-off frequency at $\omega=cq=\bar{\omega}_B$. For a finite value of τ, the rectangular spectrum has a weak Lorentzian tail. It is interesting to point out that a broad, shifted-peak structure still exists for $(\mathrm{Kn_R}, \mathrm{Kn_N})=(100, 10)$ as we show in Fig. 6. This broad shifted peak is not due to *thermalized* second sound, but due to an unequilibrated modulation of number density of phonons. The scattering mechanism in this ballistic regime is better stated as TPDS rather than light scattering by collective excitation of phonons such as thermal diffusion or second sound. TPDS can give rise to a shifted-peak structure as that shown in Fig. 6 also when the group velocity of phonons has directional dependence, i.e., when there is elastic anisotropy, as reported by Farhi *et al.*[38,47] for the low-temperature light-scattering spectrum observed in $KTaO_3$. We note that the directional dependence of

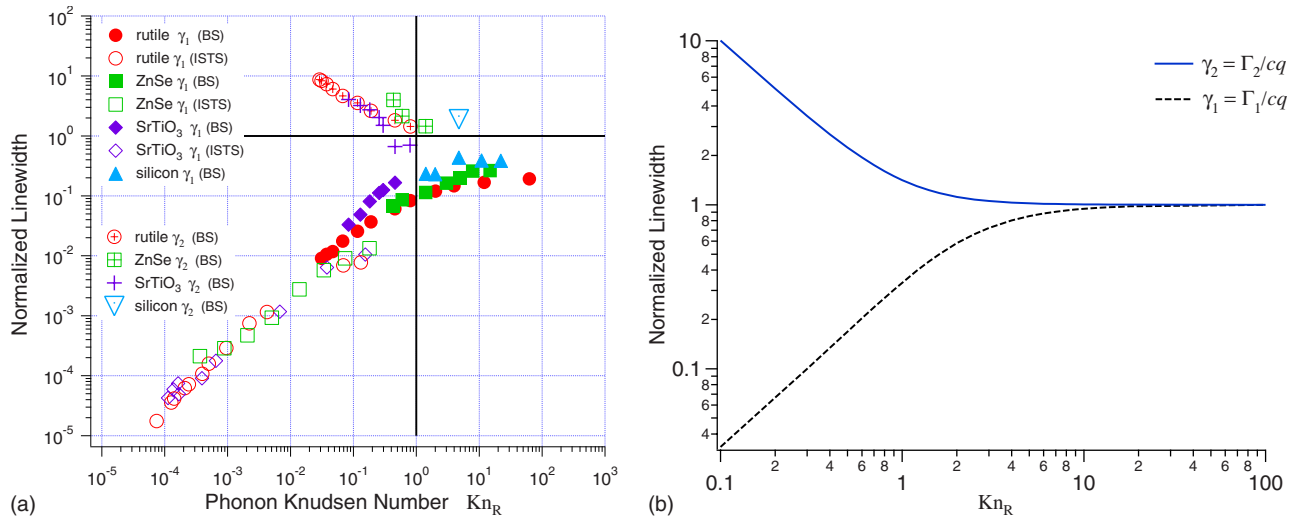

FIG. 7. (Color online) Kn_R dependence of the normalized linewidths. γ_1 and γ_2 are the normalized half widths at half maximum of the spectra of S_1 and S_2, respectively. (a) Experimentally measured Kn_R dependence of the normalized linewidths reported in Ref. 7. The BS and ISTS represent backscattering and impulsive stimulated thermal scattering, respectively. (b) Calculated linewidths of S_1 and S_2.

the pair width can also affect the line shape in the ballistic regime; in fact, the shifted-peak structure that is shown in Fig. 6 appears due to the frequency dependence of the linewidths of the "comb teeth" (those shown in Fig. 4) although an isotropic phonon dispersion is assumed.

III. COMPARISON WITH EXPERIMENTAL RESULTS

Quasielastic light-scattering spectra due to phonon-gas fluctuations have been reported in many crystals.[7,40,42,48,49] In this section, we analyze the experimental spectra with the formula given in Sec. II F. In most of the following part, we use the approximated spectral function as follows:

$$S(q,\omega) = P_1 S_1(q,\omega) + P_2 S_2(q,\omega), \tag{54}$$

with

$$S_1(q,\omega) = \frac{2cq}{\pi} \frac{\omega_0^2[\gamma_3'(q,\omega) + 1/\tau_R]}{[\omega_0^2 - \omega^2 - \omega\gamma_3''(q,\omega)]^2 + \omega^2[\gamma_3'(q,\omega) + 1/\tau_R]^2}, \tag{55}$$

$$S_2(q,\omega) = \frac{1}{\pi}[\tan^{-1}(\omega + cq)\tau - \tan^{-1}(\omega - cq)\tau], \tag{56}$$

where $\gamma_3'(q,\omega)$ and $\gamma_3''(q,\omega)$ are defined in Eqs. (31) and (32), respectively. The approximation defined in Eq. (19) has been also employed. The integrated intensities of S_1 and S_2 are given by $2cqP_1$ and $2cqP_2$, respectively, so that its ratio is given by P_1/P_2. Although P_1/P_2 is expected to be constant for a simple phonon-gas model, it will turn out to be strongly temperature dependent in practical systems. Equation (54) should be able to reproduce spectra in any phonon regime from hydrodynamic to ballistic regimes.

In the observed spectra, which will be shown later in this section, sharp Brillouin peaks due to the first-order light scattering from LA and TA acoustic phonons are present. However, it should be noted that, as we mentioned in Sec. II B, the spectral expressions derived from the ET equations essentially describes the second-order light scattering, for which the second terms on the right-hand sides of Eqs. (6) and (7) are responsible. Therefore, our spectral formula is not expected to contain those first-order contributions (Brillouin scattering) which arise from the first terms on the right-hand sides of Eqs. (6) and (7).

We have recently reported the Kn_R dependence of the normalized linewidths of the two quasielastic components measured in several crystals[7] as reproduced in Fig. 7(a). We can now simulate the Kn_R dependence of the normalized widths of S_1 and S_2, viz., Γ_1/cq and Γ_2/cq. The result is shown in Fig. 7(b): good agreement between the (a) observation and (b) theory has been found. For sufficiently small values of Kn_R, Γ_1/cq and Γ_2/cq are proportional to Kn_R and Kn_R^{-1}, respectively, indicating that Γ_1 is proportional to q^2 and that Γ_2 is independent of q in the hydrodynamic regime. Here note that Γ_1 is exactly equal to Γ_{th}, the half width of the diffusive central peak, in the hydrodynamic regime. For small Kn_R, we also see in Figs. 7(a) and 7(b) that Eq. (43) and (44) are reasonably satisfied. For sufficiently large values of Kn_R, both Γ_1/cq and Γ_2/cq are independent of Kn_R, indicating that both Γ_1 and Γ_2 are proportional to q in the ballistic limit.

In the following sections, we present fits of the obtained theoretical formula to the spectra observed in crystals of rutile (TiO_2) (Refs. 7 and 42) and strontium titanate ($SrTiO_3$).[7,50]

A. Rutile (TiO_2)

In rutile, we observed temperature dependences of the quasielastic light scattering (QELS) consisting of two components.[7,42] Figure 8 shows the temperature dependence of the spectrum observed in rutile on doubly logarithmic scales.

At high temperatures, the double-Lorentzian structure as that simulated and shown in Fig. 5 is clearly seen. The nar-

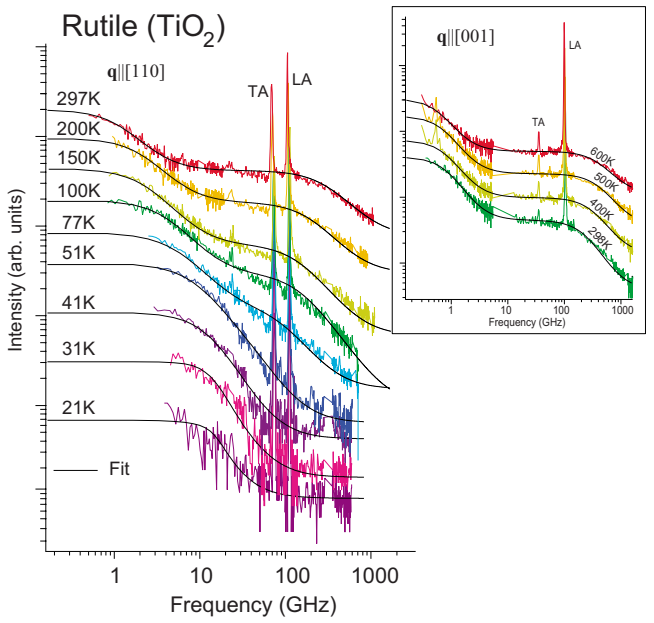

FIG. 8. (Color online) Temperature dependence of the quasielastic light-scattering spectrum observed in rutile ($\boldsymbol{q}\|[110]$). "LA" and "TA" denote longitudinal and transverse acoustic Brillouin lines, respectively. The inset shows the spectra at high temperatures ($\boldsymbol{q}\|[001]$). The solid lines are the fit of Eq. (54).

row QELS shows a q^2 dependence for the linewidth whereas the broad QELS shows no dependence on q for the linewidth.[40,42] As the temperature decreases, the narrower quasielastic component broadens and the broader one narrows; the two QELS's have opposite temperature dependences for their linewidths. This double-Lorentzian spectrum is completely consistent with the simulated spectra shown in Fig. 5, and we see that the temperature range $T \gtrsim 300$ K corresponds to the diffusion limit, viz., $\mathrm{Kn_R} \ll 1$.

At around 77 K, the linewidths of the two quasielastic components are so close as it appears that there is only one quasielastic component. Below ~50 K, the temperature dependence of the linewidth becomes weaker. Note that the constant background appearing in the low-temperature spectra is largely due to the dark counts of the photomultiplier tube employed in the experiment. In rutile, the quasielastic component does not develop into an inelastic doublet as that observed in $SrTiO_3$ (Refs. 8 and 50) as we will describe in the Sec. III B.

In fitting the spectra in rutile, we adjusted P_1, P_2, c, τ_R, and a constant background. At low temperatures, namely, $T \leq 51$ K, the fit result was better if we fix τ_R to the value estimated from known D_{th}, viz., $\tau_R = 3D_{th}/v_D^2$, where v_D is the Debye's average sound velocity. Also, at such low temperatures, a τ_N of $\sim 6 \times 10^{-11}$ s was helpful to reproduce the spectral shape although we could not determine τ_N by setting it as an adjustable parameter. The solid lines in Fig. 8 are fits of Eq. (54). The fits were quite successful in a wide range of temperature from 21 to 600 K, regardless of the simplification that employs an average sound velocity c and an average collision interval τ for LA and TA modes.

The parameters obtained by fit in rutile are listed in Table I. The spectra at relatively high temperatures were well fitted by setting all of P_1, P_2, c, and τ_R as adjustable parameters. For such high-temperature data, we did not determine τ_N because the fit was not sensitive to τ_N. It is seen that c ranges from 1500 to 3200 m/s, which is slower than the Debye velocity of $v_D \approx 6000$ m/s in rutile. This small average velocity seems to be due to the use of the common c and τ for different phonon modes, i.e., for LA and TA modes. In fact, the spectra can also be well fitted if we distinguish $c_{(l)}$ and $c_{(t)}$, and $\tau^{(l)}$ and $\tau^{(t)}$, where $c_{(l)}$ and $c_{(t)}$ were measured directly from the Brillouin frequency in the scattered spectra. The integrated intensities of S_1 and S_2 are also listed in Table I. The results are similar to those we reported previously.[42] Note that the intensity ratio P_1/P_2 is very small at high temperatures, and it increases on cooling, indicating that the viscosity in the phonon gas (the contributions to P_2) is larger at high temperatures and it decreases with decreasing temperature.

We estimated the thermal diffusivity from the relation, $D_{th} = \frac{1}{3}c^2\tau_R$, and compared it with the values calculated from

TABLE I. Parameters obtained by fitting in rutile. The bracketed values were fixed in fitting.

T (K)	τ_R (s)	τ_N (s)	c (m/s)	P_1	P_2
600	3.6×10^{-13}		2800	1.21	124
500	3.5×10^{-13}		3200	1.53	113
400	4.6×10^{-13}		2900	1.70	93.1
298	6.5×10^{-13}		2500	2.54	78.1
297	5.3×10^{-13}		3100	1.85	61.2
200	8.5×10^{-13}		3200	2.38	24.6
150	1.2×10^{-12}		2900	3.88	16.5
101	2.1×10^{-12}		2800	2.44	5.22
77	2.8×10^{-12}	(6×10^{-11})	2800	1.90	1.99
51	(1.0×10^{-11})	(6×10^{-11})	1800	1.10	0.928
41	(3.8×10^{-11})	(6×10^{-11})	2100	0.580	0.351
31	(1.4×10^{-10})	(6×10^{-11})	1500	0.00938	0.375
21	(1.5×10^{-9})	4×10^{-11}	2100	0.00	0.108

TABLE II. Temperature dependence of the thermal diffusivity (D_{th}) in rutile. $D_{\mathrm{th}}^{(\mathrm{lit})}$'s were calculated from the literature values of thermal conductivity (κ) and specific heat (C_p) with the relation $D_{\mathrm{th}}=\kappa/\rho C_p$. For the values for T=51, 41, 31, and 21 K, τ_{R} was estimated from $D_{\mathrm{th}}^{(\mathrm{lit})}$.

T (K)	$D_{\mathrm{th}}^{(\mathrm{lit})}$ (m^2/s)	$\frac{1}{3}c^2\tau_{\mathrm{R}}$ (m^2/s)
600	1.1×10^{-6}	9.4×10^{-7}
500	1.4×10^{-6}	1.2×10^{-6}
400	1.8×10^{-6}	1.3×10^{-6}
300	2.6×10^{-6}	1.7×10^{-6}
200	4.3×10^{-6}	2.9×10^{-6}
150	7.0×10^{-6}	3.4×10^{-6}
101	1.7×10^{-5}	5.5×10^{-6}
77	3.4×10^{-5}	7.3×10^{-6}
51	1.3×10^{-4}	1.1×10^{-5}
41	3.8×10^{-4}	5.6×10^{-5}
31	1.7×10^{-3}	1.1×10^{-4}
21	2.0×10^{-2}	2.2×10^{-3}

the known values of thermal conductivity[51] (κ) and specific heat[52] (C_p) with the relation $D_{\mathrm{th}}=\kappa/\rho C_p$, where ρ is the mass density. The values are listed in Table II. Good agreement was found at relatively high temperatures. Although the agreement is not so good at relatively low temperatures due to the small c, the deviations were approximately one order, which seems to be reasonable for the present simplification of the model.

B. $SrTiO_3$

$SrTiO_3$ is well known as a kind of perovskite-type crystals. Many of other perovskite-type crystals such as $BaTiO_3$ is known to undergo displacive-type ferroelectric phase transition when they are cooled down to their Curie temperature because of freezing of an optical phonon mode ("soft mode") that corresponds to the polarizable displacement of the ions.[53] Although $SrTiO_3$ does have such a soft optical phonon mode, the relatively large quantum fluctuation is thought to disturb the freezing of the soft mode in $SrTiO_3$,[54] forcing it to stay in paraelectric phase, and hence, $SrTiO_3$ is referred to as a "quantum paraelectric.[55]" In $SrTiO_3$, an anomalous Brillouin doublet was reported by Hehlen *et al.*,[8] and they proposed that the origin of the new Brillouin doublet was the second sound according to the theoretical prediction by Gurevich and Tagantsev.[9] In addition, the molecular dynamics studies published earlier by Schneider and Stoll[11,12] had clearly indicated the existence of second sound in a model of displacive-type ferroelectric with an optical phonon mode that softens in the Brillouin-zone center. We have observed that the thermal-Rayleigh central peak changed into the new Brillouin spectrum on cooling,[7] and pointed out the possibility of the existence of the second sound in $SrTiO_3$, supporting the proposal made by Hehlen *et al.* More recently, we have reported an ET analysis of the spectra in $SrTiO_3$,[50,56] and we have shown that the overdamped thermal wave (thermal diffusion) is actually underdamped in a narrow temperature range around 30 K. Figure 9 shows the temperature variation in the low-frequency light-scattering spectrum in $SrTiO_3$. Although we have employed a more rigorous, but complicated form for the spectral expression [Eq. (3) in Ref. 50], we have confirmed that fitting Eq. (54) for all the investigated temperatures give almost the same results as the analysis we reported in Ref. 50.

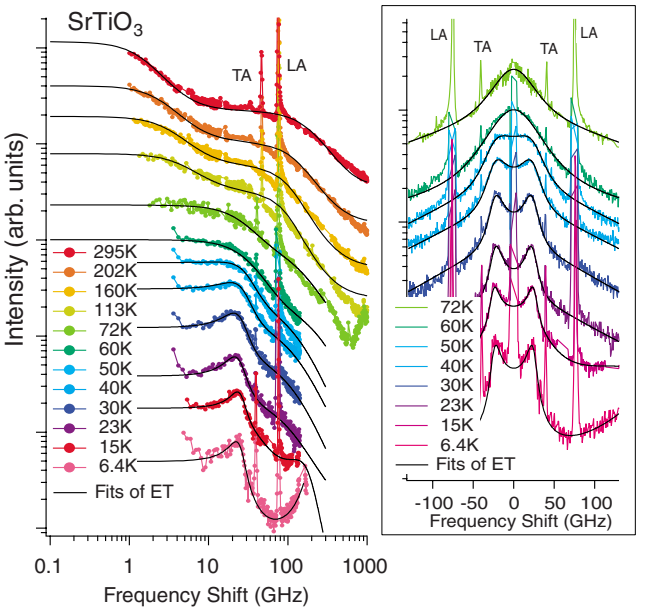

FIG. 9. (Color online) Temperature dependence of the low-frequency light-scattering spectra in $SrTiO_3$ from 6 to 295 K (log-log plot). The LA and TA denotes longitudinal and transverse acoustic phonons' Brillouin lines, respectively. The inset is a semi-log plot for the spectra below 72 K. Each spectrum is appropriately scaled for visual clarity. The solid lines are fits of Eq. (54).

Figure 10 shows the temperature dependences of the obtained τ_{N}, ω_{ss}, and Γ_{ss}.[50] The expressions for ω_{ss} and Γ_{ss} in

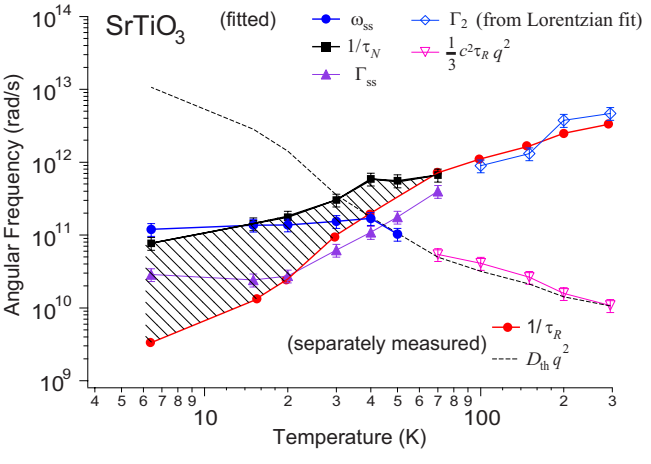

FIG. 10. (Color online) Temperate dependences of the normal (τ_{N}^{-1}) and the resistive (τ_{R}^{-1}) phonon relaxation rates in $SrTiO_3$. Legends are shown in the figure. All the lines between the symbols are guides to the eyes. The dashed horizontal line at $\sim2\times10^{11}$ rad/s represents a constant $qv_{\mathrm{D}}/\sqrt{3}\approx\omega_0$. The shaded area indicates the "window" for second-sound propagation.

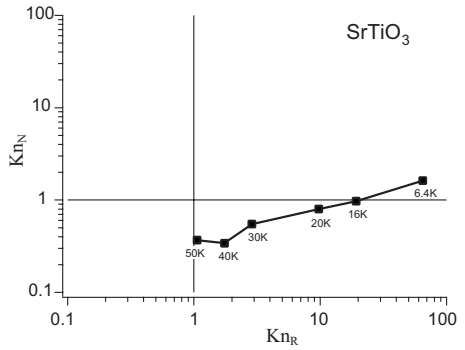

FIG. 11. Phonon Knudsen numbers measured in $SrTiO_3$ (the closed squares). See Figs. 2 and 5 for qualitative comparison.

terms of τ_N, τ_R are defined in Eqs. (34) and (36), respectively. The values of τ_R were measured in a separate work[7] except for the value at 6.4 K, which could not be determined from the employed experimental condition in the work; τ_R for 6.4 K was estimated from literature values of κ and C_p with Eq. (40). The shaded area in Fig. 10 is the "open window" for second-sound propagation, where $\tau_R^{-1} < \tau_N^{-1}$. If the second-sound frequency, ω_{ss}, enters into that area, then underdamped second sound is expected to propagate. Indeed, the obtained ω_{ss} lies in the shaded area in the temperature range approximately between 20 and 30 K as can be seen in Fig. 10.

At higher temperatures than ~30 K, the second sound is overdamped because $\omega_{ss} < \tau_R^{-1}$, resulting in the quasielastic scattering observed for $T \gtrsim 40$ K. At much higher temperatures, the damping is strong enough to regard the overdamped thermal wave as "diffusion of heat," and the spectrum consists of a narrow thermal Rayleigh mode and the broad Mountain mode. Indeed, as can be seen in Fig. 10, the estimated D_{th} and fitted τ_R well reproduce the reported values of D_{th} and τ_R, respectively. This double QELS structure is equivalent to what was observed in rutile at high temperatures, as shown in the Sec. III A. At lower temperatures than ~15 K, the second sound cannot be defined any more because $\tau_N^{-1} < \omega_{ss}$, i.e., there are too few phonon collisions during a period of the second-sound oscillation. Even in such a case, however, light-scattering spectrum can exhibit inelastic peaks as we have shown in Fig. 5. Therefore, we should consider that scattering mechanism for the inelastic peaks observed at 6.4 K in $SrTiO_3$ is TPDS on the same phonon branch[38] rather than second sound.

We can review how the phonon regime changed in $SrTiO_3$ according to the temperature by plotting the phonon Knudsen numbers in the (Kn_R, Kn_N) plane. Figure 11 shows the temperature dependence of the point (Kn_R, Kn_N). It is seen that $SrTiO_3$ under the investigated condition ($q = 6.0 \times 10^7$ 1/m) actually goes out of the thermal-diffusion regime at around 50 K, then, enters into the second-sound regime around 30 K, and finally goes out to the ballistic regime at the lowest temperature.

IV. DISCUSSIONS

In the previous section, we confirmed that the two-component QELS (double QELS) arises from the overdamped thermal waves (the narrow QELS) and their interaction phenomenon (the broad component). In $SrTiO_3$, the thermal wave was found to be underdamped below 40 K, and the narrower QELS changed into a broad-doublet spectrum. Our analysis showed that ω_{ss} was in the narrow "second-sound window," and the broad doublet in $SrTiO_3$ could be attributed to the second sound in the hydrodynamic regime.

The physical origin of the broad doublet in $SrTiO_3$ has been a long standing controversy.[8,55,57–59] Hehlen *et al.* were the first to report the extra Brillouin doublet in $SrTiO_3$, and they tentatively proposed that the new doublet was due to the second sound according to the theory of Gurevich and Tagantsev.[9] However, Scott *et al.*[59] have published a number of negative reports and they argued that the new doublet should be arising from the light scattering from two-phonon difference processes on two optical phonon branches that accidentally degenerate at ~37 K. Scott *et al.* claimed that the light-scattering intensity for the second sound (entropy fluctuations) should be much weaker than predicted although they did not show a quantitative discussion on this aspect. However, our observation and analysis have revealed that the previously reported[7,40] narrow QELS due to thermal diffusion (entropy fluctuations) survives even at a temperature as low as 50 K. Furthermore, at even lower temperatures, the narrow QELS gradually changes its shape into a shifted doublet with smooth changes in the line-shape-determining parameters, namely, τ_R, τ_N, and ω_{ss}, as shown in Fig. 10.

We also emphasize that the simultaneous existence of the broader QELS and the broad doublet is also a sign of the second sound. Our simulation for the spectrum (Fig. 5) indicates that the second-sound doublet should be superposed on the broader QELS (Mountain mode), which was actually observed in the experiments.[7,8,50,60] The fact that the fitted τ_N, c, and the known τ_R reproduced the entire spectral shape implies the high reliability of our analysis. In fact, the values obtained for c ranged from 3600 m/s at 6.4 K to 5900 m/s at 50 K, which are quite reasonable compared with $v_D = 5400$ m/s, where v_D is the average sound velocity in the Debye's theory. The value of τ_N can be roughly evaluated from the Gurevich-Tagantsev relation,[9]

$$\frac{\tau_U}{\tau_N} \sim \epsilon^{1/2},$$

where τ_U and ϵ are the umklapp-scattering time and the dielectric constant, respectively. Replacing τ_U with τ_R, which is smaller than τ_U in general, and substituting the known value for ϵ [$\sim 10^{3-4}$ for $T \sim 20$ K (Ref. 61)], $1/\tau_N$ is expected to be on the order of 10^{12} rad/s or less for $T \sim 20$ K; this does not contradict our result.

Tsujimi and Itoh[62] have published another interpretation for the broad doublet. Their hypothesis is that the broad doublet is arising from the partially softened TA phonon in the small polar regions, which are thought to exist in $SrTiO_3$.[63,64] They have shown that significant doping of cations killed the broad doublet in $SrTiO_3$, and they argued that the screening by the doped cations disturbed the development of small polar regions and that it in turn killed the softened TA phonons, which could otherwise exist locally in the small polar region. Since such polar regions contain softened TO

phonons of low energy, the normal phonon collisions that are necessary for the second-sound excitation should also be enhanced in such local regions because normal phonons should have low energy.[9] Therefore, the reported disappearance of the broad doublet in doped samples of $SrTiO_3$ cannot rule out the second-sound scenario. Tsujimi and co-workers[60] fitted a formula consisting of a spectrum for damped harmonic oscillator and a broad central Lorentzian to the observed spectra, but the fitted formula employed at least six unknown parameters, while our analysis had only five; τ_N, ω_{ss}, P_1, P_2, and the baseline. Furthermore, the widths for the fitted damped harmonic oscillator and QELS in their analysis could be adjusted independently, whereas S_1 and S_2 in our ET formula involve common line-shape determining parameters, namely, τ_N and τ_R, i.e., the two components, S_1 and S_2, have mutually dependent linewidths.

In $KTaO_3$, which is thought as a similar system to $SrTiO_3$, an extra Brillouin doublet very similar to that in $SrTiO_3$ has also been reported below ~15 K.[8,38] The origin of the new doublet in $KTaO_3$ was first proposed to be due to second sound,[8] then later reinvestigated by Farhi *et al.*,[38,65] who have shown a possibility that such a broad doublet could arise also from two-phonon difference processes on a single phonon branch if there is elastic anisotropy. In our analysis for $SrTiO_3$, the temperature of 6.4 K corresponds to the ballistic regime as we showed in Fig. 11. Thus, the scattering process for the low-temperature doublet should be viewed as arising from the TPDS on the same phonon branch, rather than as arising from hydrodynamic second sound, as we pointed out in Sec. III. The doubletlike line shape is obtained also in our model if we assume a frequency dependence for the pair width for an isotropic phonon dispersion: this is compatible with the analysis by Farhi *et al.*

In the present theory, the temperature dependence of the integrated intensities for both S_1 and S_2 components have not been given. Also, the observed intensity ratio between the two components, namely, P_1/P_2, was strongly temperature dependent, which is not predicted in the present theory. These issues concerning the intensities might be resolved, for instance, by properly including one-phonon (Brillouin) scattering, whose intensity is connected with the intensity of $S_1(q,\omega)$ through the modified Landau-Placzek ratio,[18] and it would also enable reproduction of the interference between the Brillouin peaks and the broader QELS as seen in Fig. 9 as the asymmetry of the LA Brillouin lines.[7,8,42]

V. SUMMARY

We calculated light-scattering spectra in a phonon gas from ET equations of Dreyer and Struchtrup.[14] Since the ET-equation set is applicable not only in hydrodynamic regime but also in collisionless regime, the obtained spectral formula can be used in any regime, i.e., in a wide range of temperature and magnitude of q.

The spectral formula consists of two parts, namely, the thermal-wave term and the interaction term according to the basing ET-equation set, which can be interpreted as a coupled wave equation for the second sounds in the LA and TA phonon gases. Thus, the two spectral components could be interpreted as arising from the two normal modes in the coupled wave-equation system. The thermal-wave term yields either central peak or broad doublet in the scattering spectrum according to whether the thermal wave is overdamped or underdamped. The interaction term always yields a central peak whose linewidth is equal to the rate of collisions between the thermal phonons. Since, in the hydrodynamic regime, the phonon-collision rate is much higher than the rate of thermal diffusion and than the frequency of first sound, the latter quasielastic component has much broader width than that of the former component or the Brillouin shift. This broad QELS can alternatively interpreted as the so-called "Mountain mode" because the spectrum comes from the interaction between the second sounds via the nonequilibrium viscosity in the phonon gas.

As the ballistic regime is approached, the two spectral components develops into the same form, which is a rectangular spectrum in the limit of the ballistic regime. In the ballistic limit, both spectral components exhibit q-linear dependence for the linewidth, which is in complete contrast to the q^2 and q^0 dependences in the hydrodynamic regime for the narrow and broad QELS's, respectively. We showed that the spectrum in the ballistic regime could alternatively be constructed from the two-phonon difference light-scattering processes concerning two phonons on the same dispersion branch, and that the spectral formula obtained from ET and TPDS coincides with each other in the ballistic limit.

We fitted the spectral formula obtained from ET to the spectra experimentally observed in rutile and $SrTiO_3$. We found good agreements between the fitted parameters and the literature values available. In particular, the temperature dependence of τ_N in $SrTiO_3$ was determined, and it indicated the existence of the second-sound excitation in the narrow temperature range around 30 K.

ACKNOWLEDGMENTS

This research was partially supported by The Murata Science Foundation (for A.K.), and by the Japan Ministry of Education, Science, Sports and Culture, Grant-in-Aid for Young Scientists B (for A.K.), Grant No. 18740171 and 21740218.

APPENDIX A: CONTINUED FRACTION EXPANSION OF THE SPECTRAL FUNCTION

Here we seek direct solutions of Eqs. (A1) for fluctuation spectra of $e^{(l)}$ and $e^{(t)}$, rather than those of normal modes. We first perform Fourier-Laplace transform for Eqs. (1) and (2). The resulting equations can be written in a matrix form as the following:

$$\boldsymbol{M}\cdot\boldsymbol{v}=\boldsymbol{v}_0, \tag{A1}$$

where $\boldsymbol{M}$, $\boldsymbol{v}$, and $\boldsymbol{v}_0$ have been defined as

$$\boldsymbol{M}\equiv\begin{bmatrix}\boldsymbol{L} & \boldsymbol{A}\\ \boldsymbol{A}' & \boldsymbol{T}\end{bmatrix},\quad \boldsymbol{v}\equiv\begin{bmatrix}\boldsymbol{v}_l\\ \boldsymbol{v}_t\end{bmatrix},\quad \boldsymbol{v}_0\equiv\begin{bmatrix}\boldsymbol{v}_{l0}\\ \boldsymbol{v}_{t0}\end{bmatrix}.$$

Here $\boldsymbol{L}$, $\boldsymbol{T}$, $\boldsymbol{A}$, $\boldsymbol{A}'$, $\boldsymbol{v}_l$, and $\boldsymbol{v}_t$ are block matrices defined as the followings:

$$\boldsymbol{L} \equiv \begin{bmatrix} s+2Ac_{(t)}^3 & ic_{(l)}q & 0 & 0 & \cdots \\ i\alpha_2 c_{(l)}q & s+1/\tau_{\mathrm{R}}^{(l)}+2Bc_{(t)}^5 & ic_{(l)}q & 0 & \cdots \\ 0 & i\alpha_3 c_{(l)}q & s+1/\tau^{(l)} & ic_{(l)}q & \cdots \\ 0 & 0 & i\alpha_4 c_{(l)}q & s+1/\tau^{(l)} & \cdots \\ \cdots & \cdots & \cdots & \cdots & \cdots \end{bmatrix},$$

$$\boldsymbol{T} \equiv \begin{bmatrix} s+Ac_{(l)}^3 & ic_{(l)}q & 0 & 0 & \cdots \\ i\alpha_2 c_{(t)}q & s+1/\tau_{\mathrm{R}}^{(t)}+Bc_{(t)}^5 & ic_{(t)}q & 0 & \cdots \\ 0 & i\alpha_3 c_{(t)}q & s+1/\tau^{(t)} & ic_{(t)}q & \cdots \\ 0 & 0 & i\alpha_4 c_{(t)}q & s+1/\tau^{(t)} & \cdots \\ \cdots & \cdots & \cdots & \cdots & \cdots \end{bmatrix},$$

$$\boldsymbol{A} \equiv \begin{bmatrix} -2Ac_{(t)}^3 & 0 & 0\cdots \\ 0 & -2Bc_{(t)}^5 & 0\cdots \\ 0 & 0 & 0\cdots \\ \cdots & \cdots & \cdots \end{bmatrix}, \quad \boldsymbol{A}' \equiv \begin{bmatrix} -Ac_{(l)}^3 & 0 & 0\cdots \\ 0 & -Bc_{(l)}^5 & 0\cdots \\ 0 & 0 & 0\cdots \\ \cdots & \cdots & \cdots \end{bmatrix},$$

$$\boldsymbol{v}_l \equiv [e^{(l)}(q,s),p^{(l)}(q,s),\ldots]^T, \quad \boldsymbol{v}_t \equiv [e^{(t)}(q,s),p^{(t)}(q,s),\ldots]^T,$$

$$\boldsymbol{v}_{l0} \equiv [e^{(l)}(q,0),p^{(l)}(q,0),\ldots]^T, \quad \boldsymbol{v}_{t0} \equiv [e^{(t)}(q,0),p^{(t)}(q,0),\ldots]^T,$$

where the wave vector $\boldsymbol{q}$ must be considered as the wave-vector transfer in light-scattering experiments, viz., $q=(2\pi\eta/\Lambda)\sin(\theta/2)$, where η, Λ, and θ are the refractive index, the light wavelength, and the scattering angle, respectively.

1. Uncoupled case (independent gases)

First we consider LA and TA modes without interaction with the other modes. Setting $A=B=0$, we obtain a subsystem of Eq. (A1) as

$$\boldsymbol{L}\cdot\boldsymbol{v}_l = \boldsymbol{v}_{l0} \tag{A2}$$

or

$$\boldsymbol{T}\cdot\boldsymbol{v}_t = \boldsymbol{v}_{t0}. \tag{A3}$$

This system can be regarded as independent or pure phonon gases, which do not interact with other modes and no energy exchange exists. In this case, all we have to do is solve each of Eqs. (A2) and (A3) separately. Each of the subsystems is quite similar to that appears in the analysis of ladder-type electrical circuits.[66,67] The present system corresponds to a coupled case of two ladder-type circuits, and the solutions can be expressed as combinations of the solutions for the subsystems.

To obtain the spectrum for mode λ, we calculate a quantity $\langle e^{(\lambda)^*}(q,0)e^{(\lambda)}(q,s)\rangle$. Thus we may set $\boldsymbol{v}_0=[e^{(\lambda)}(q,0),0,0,\ldots]$ because of the mutual independence of the variables in each phonon gas.[5] It is easily found that in the independent subsystems Eqs. (A2) and (A3),

$$e^{(l)}(q,s) = (\boldsymbol{L}^{-1})_{11}e^{(l)}(q,0) = \frac{\det \boldsymbol{Q}^{(l)}}{\det \boldsymbol{L}}e^{(l)}(q,0) \tag{A4}$$

$$e^{(t)}(q,s) = (\boldsymbol{T}^{-1})_{11}e^{(t)}(q,0) = \frac{\det \boldsymbol{Q}^{(t)}}{\det \boldsymbol{T}}e^{(t)}(q,0), \tag{A5}$$

where $\det \boldsymbol{m}$ denotes the determinant of a matrix $\boldsymbol{m}$, and $\det \boldsymbol{Q}^{(l)}$ and $\det \boldsymbol{Q}^{(t)}$ are the $i=j=1$ components of the cut matrices for submatrices $\boldsymbol{L}$ and $\boldsymbol{T}$, respectively. Therefore, $\boldsymbol{Q}^{(l)}$ and $\boldsymbol{Q}^{(t)}$ are obtained by deleting the first row and the first column from $\boldsymbol{L}$ and $\boldsymbol{T}$, respectively. The determinants in Eq. (A4) satisfy the following recursive relations:

$$\frac{\det \boldsymbol{Q}_i^{(l)}}{\det \boldsymbol{L}_i} = \frac{\boldsymbol{L}_{ii}\det \boldsymbol{Q}_{i-1}^{(l)} + \alpha_i c_{(l)}^2 q^2 \det \boldsymbol{Q}_{i-2}^{(l)}}{\boldsymbol{L}_{ii}\det \boldsymbol{L}_{i-1} + \alpha_i c_{(l)}^2 q^2 \det \boldsymbol{L}_{i-2}}, \quad (n \geq 2), \tag{A6}$$

where we have written a matrix with $i\times i$ components as $\boldsymbol{m}_i$. We write Eq. (A6) in a matrix form as

$$\begin{bmatrix} \det \boldsymbol{Q}_i^{(l)} \\ \det \boldsymbol{L}_i \end{bmatrix} = \boldsymbol{G}_{i-1}\begin{bmatrix} \boldsymbol{L}_{ii} \\ \alpha_i c_{(l)}^2 q^2 \end{bmatrix} \tag{A7}$$

$$\text{with } \boldsymbol{G}_{i-1} \equiv \begin{bmatrix} \det \boldsymbol{Q}_{i-1}^{(l)} & \det \boldsymbol{Q}_{i-2}^{(l)} \\ \det \boldsymbol{L}_{i-1} & \det \boldsymbol{L}_{i-2} \end{bmatrix}. \tag{A8}$$

This method is known as "Möbius transformation" or linear fractional transformation. We find that the matrix $\boldsymbol{G}_{i-1}$ can be factorized as

$$\begin{aligned} \boldsymbol{G}_{i-1} &= \boldsymbol{G}_{i-2} \begin{bmatrix} L_{i-1,i-1} & 1 \\ \alpha_{i-1} c_{(l)}^2 q^2 & 0 \end{bmatrix} \\ &= \boldsymbol{G}_{i-3} \begin{bmatrix} L_{i-2,i-2} & 1 \\ \alpha_{i-2} c_{(l)}^2 q^2 & 0 \end{bmatrix} \begin{bmatrix} L_{i-1,i-1} & 1 \\ \alpha_{i-1} c_{(l)}^2 q^2 & 0 \end{bmatrix} \\ &= \boldsymbol{G}_1 \boldsymbol{H}_2 \boldsymbol{H}_3 \cdots \boldsymbol{H}_{i-1}, \end{aligned}$$

where

$$\boldsymbol{H}_i \equiv \begin{bmatrix} L_{ii} & 1 \\ \alpha_i c_{(l)}^2 q^2 & 0 \end{bmatrix},$$

and

$$\boldsymbol{G}_1 = \begin{bmatrix} \det \boldsymbol{Q}_1^{(l)} & \det \boldsymbol{Q}_0^{(l)} \\ \det \boldsymbol{L}_1 & \det \boldsymbol{L}_0 \end{bmatrix} = \begin{bmatrix} 1 & 0 \\ L_{11} & 1 \end{bmatrix}.$$

Hence we see that

$$\begin{bmatrix} \det \boldsymbol{Q}_n^{(l)} \\ \det \boldsymbol{L}_n \end{bmatrix} = \boldsymbol{G}_1 \boldsymbol{H}_2 \boldsymbol{H}_3 \cdots \boldsymbol{H}_{n-1} \begin{bmatrix} L_{nn} \\ \alpha_n c_{(l)}^2 q^2 \end{bmatrix}.$$

We note here that the operation of $\boldsymbol{H}_{i-1}$ to a vector $[L_{ii}, \alpha_i c_{(l)}^2 q^2]^T$, i.e., to a fraction $\frac{L_{ii}}{\alpha_i c_{(l)}^2 q^2}$, yields a new fraction of the form

$$\frac{1}{\alpha_{i-1} c_{(l)}^2 q^2} \left(L_{i-1,i-1} + \frac{\alpha_i c_{(l)}^2 q^2}{L_{ii}} \right) \equiv \frac{1}{\alpha_{i-1} c_{(l)}^2 q^2} \frac{1}{\gamma_{i-1}},$$

where γ_i has been introduced as

$$\gamma_i \equiv \frac{1}{L_{ii} + \alpha_{i+1} c_{(l)}^2 q^2 \gamma_{i+1}}, \tag{A9}$$

which is the recursive relation for γ_i. For an n-moment system, $\gamma_{n+1}=0$ because of the closure theorem.[14] Successive operations of $\boldsymbol{H}_i$, i.e., $\Pi_{i=2}^{n-1} \boldsymbol{H}_i$, yields a continued fraction of the form

$$\frac{1}{\gamma_2} = L_{22} + \cfrac{\alpha_3 c_{(l)}^2 q^2}{L_{33} + \cfrac{\alpha_4 c_{(l)}^2 q^2}{L_{44} + \cfrac{\alpha_5 c_{(l)}^2 q^2}{L_{55} + \cdots}}}.$$

Since the last operator $\boldsymbol{G}_1$ transforms a fraction $1/(\alpha_2 c_{(l)}^2 q^2 \gamma_2)$ into $1/(L_{11} + \alpha_2 c_{(l)}^2 q^2 \gamma_2) = \gamma_1$, the right-hand side of Eq. (A7) can be expressed in a continued fraction form as

$$\frac{\det \boldsymbol{Q}_n^{(l)}}{\det \boldsymbol{L}_n} = \gamma_1^{(l)} = \cfrac{1}{L_{11} + \cfrac{\alpha_2 c_{(l)}^2 q^2}{L_{22} + \cfrac{\alpha_3 c_{(l)}^2 q^2}{L_{33} + \cdots}}}.$$

A completely analogous discussion can be made for the TA mode, and we obtain from Eq. (A5) that

$$\frac{\det \boldsymbol{Q}_n^{(t)}}{\det \boldsymbol{T}_n} = \gamma_1^{(t)} = \cfrac{1}{T_{11} + \cfrac{\alpha_2 c_{(t)}^2 q^2}{T_{22} + \cfrac{\alpha_3 c_{(t)}^2 q^2}{T_{33} + \cdots}}}.$$

Thus, from Eqs. (A4) and (A5), we obtain spectra in continued-fraction forms for the *pure* LA and TA phonon gases, respectively, as

$$S^{(l)}(q,s) \propto \frac{\langle e^{(l)^*}(q,0) e^{(l)}(q,s) \rangle}{\langle e^{(l)^*}(q,0) e^{(l)}(q,0) \rangle} = \gamma_1^{(l)} \tag{A10}$$

$$S^{(t)}(q,s) \propto \frac{\langle e^{(t)^*}(q,0) e^{(t)}(q,s) \rangle}{\langle e^{(t)^*}(q,0) e^{(t)}(q,0) \rangle} = \gamma_1^{(t)}. \tag{A11}$$

2. Coupled case

Next, we consider the coupling between the modes. Similarly to Eqs. (A2) and (A4), $e^{(l)}(q,s)$ can be expressed as

$$e^{(l)}(q,s) = (\boldsymbol{M}^{-1})_{11} e^{(l)}(q,0) = \frac{\det \boldsymbol{\Theta}}{\det \boldsymbol{M}} e^{(l)}(q,0),$$

where the matrix $\boldsymbol{\Theta}$ has been defined as follows:

$$\boldsymbol{\Theta} \equiv \begin{bmatrix} \boldsymbol{Q}^{(l)} & \boldsymbol{a} \\ \boldsymbol{a}' & \boldsymbol{T} \end{bmatrix},$$

with

$$\boldsymbol{a} = \begin{bmatrix} 0 & \boldsymbol{A}_{22} & 0 & \cdots \\ 0 & 0 & 0 & \cdots \\ \cdots & \cdots & \cdots & \cdots \end{bmatrix}, \quad \boldsymbol{a}' = \begin{bmatrix} 0 & 0 & \cdots \\ \boldsymbol{A}'_{22} & 0 & \cdots \\ 0 & 0 & \cdots \\ \cdots & \cdots & \cdots \end{bmatrix},$$

where $\boldsymbol{a}$ and $\boldsymbol{a}'$ are obtained by deleting the first row of $\boldsymbol{A}$ and first column of $\boldsymbol{A}'$, respectively. The determinants of the matrices $\boldsymbol{M}$ and $\boldsymbol{\Theta}$ can be calculated as

$$\det \boldsymbol{\Theta} = \det \boldsymbol{Q}^{(l)} \times \det[\boldsymbol{T} - \boldsymbol{a}' \boldsymbol{Q}^{(l)^{-1}} \boldsymbol{a}]$$

$$\det \boldsymbol{M} = \det \boldsymbol{L} \times \det[\boldsymbol{T} - \boldsymbol{A}' \boldsymbol{L}^{-1} \boldsymbol{A}].$$

Hence, we see that

$$\frac{\det \boldsymbol{\Theta}}{\det \boldsymbol{M}} = \frac{\det \boldsymbol{Q}^{(l)}}{\det \boldsymbol{L}} \times \frac{\det[\boldsymbol{T} - \boldsymbol{a}' \boldsymbol{Q}^{(l)^{-1}} \boldsymbol{a}]}{\det[\boldsymbol{T} - \boldsymbol{A}' \boldsymbol{L}^{-1} \boldsymbol{A}]} = \gamma_1^{(l)} \times \frac{\det \boldsymbol{\Phi}}{\det \boldsymbol{P}}, \tag{A12}$$

where we have defined that

$$\boldsymbol{\Phi} \equiv \boldsymbol{T} - \boldsymbol{a}'\boldsymbol{Q}^{(l)^{-1}}\boldsymbol{a}, \quad \boldsymbol{P} \equiv \boldsymbol{T} - \boldsymbol{A}'\boldsymbol{L}^{-1}\boldsymbol{A}.$$

We see in Eq. (A12) in comparison with the noninteracting spectrum of Eq. (A10) that the interacting spectrum differs by the factor $\det \boldsymbol{\Phi}/\det \boldsymbol{P}$, which includes information of the interaction between the modes. This modification factor can be computed by Möbius transformation method similarly to the earlier part of this section when $n \geq 3$, and we obtain

$$\begin{bmatrix} \det \boldsymbol{\Phi}_n \\ \det \boldsymbol{P}_n \end{bmatrix} = \begin{bmatrix} \boldsymbol{\Phi}_{11}\boldsymbol{\Phi}_{22} + \alpha_2 c_{(t)}^2 q^2 & \boldsymbol{\Phi}_{11} \\ \boldsymbol{P}_{22}\boldsymbol{P}_{11} - \boldsymbol{P}_{12}\boldsymbol{P}_{21} & \boldsymbol{P}_{11} \end{bmatrix} \begin{bmatrix} 1 \\ \alpha_3 c_{(t)}^2 q^2 \gamma_3^{(t)}. \end{bmatrix}$$

Care should be paid when $n \leq 2$ noting that

$$\boldsymbol{\Phi}_{11} = \boldsymbol{T}_{11},$$

$$\boldsymbol{\Phi}_{22} = \boldsymbol{T}_{22} - \boldsymbol{A}_{22}\boldsymbol{A}'_{22}\gamma_2^{(l)},$$

$$\boldsymbol{P}_{11} = \boldsymbol{T}_{11} - \boldsymbol{A}_{11}\boldsymbol{A}'_{11}\gamma_1^{(l)},$$

$$\boldsymbol{P}_{22} = \boldsymbol{T}_{22} - \boldsymbol{A}_{22}\mathbf{A}'_{22}\boldsymbol{L}_{11}\gamma_1^{(l)}\gamma_2^{(l)},$$

$$\boldsymbol{P}_{12} = ic_{(t)}q\left(1 + \boldsymbol{A}_{11}\boldsymbol{A}'_{22}\frac{c_{(l)}}{c_{(t)}}\gamma_1^{(l)}\gamma_2^{(l)}\right),$$

$$\text{and } \boldsymbol{P}_{21} = ic_{(t)}q\left(1 + \boldsymbol{A}_{22}\boldsymbol{A}'_{11}\frac{c_{(l)}}{c_{(t)}}\gamma_1^{(l)}\gamma_2^{(l)}\right),$$

then we obtain for $n \geq 3$

$$\frac{\det \boldsymbol{\Phi}_n}{\det \boldsymbol{P}_n} = \frac{1 - \boldsymbol{A}_{22}\boldsymbol{A}'_{22}\boldsymbol{T}_{11}\gamma_2^{(l)}\gamma_1^{(t)}\gamma_2^{(t)}}{1 - \boldsymbol{A}_{11}\boldsymbol{A}'_{11}\gamma_1^{(l)}\gamma_1^{(t)} - \gamma_1^{(l)}\gamma_2^{(l)}\gamma_1^{(t)}\gamma_2^{(t)}w^{(l)}},$$

where $w^{(l)}$ is proportional to B (the coupling constant for the momentum), and the explicit expression for $w^{(l)}$ is given later. Writing down the components of the matrices, we obtain from Eq. (A12) the interacting spectrum for mode (λ) in the Fourier-Laplace space as follows:

$$S^{(\lambda)}(q,s) \propto \frac{\langle e^{(\lambda)^*}(q,0)e^{(\lambda)}(q,s)\rangle}{\langle e^{(\lambda)^*}(q,0)e^{(\lambda)}(q,0)\rangle} = \gamma_1^{(\lambda)}\frac{1 - 2B^2c_{(\lambda)}^5c_{(\lambda')}^5(s + a^{(\lambda')}Ac_{(\lambda')}^3)\gamma_2^{(\lambda)}\gamma_1^{(\lambda')}\gamma_2^{(\lambda')}}{1 - 2A^2c_{(\lambda)}^3c_{(\lambda')}^3\gamma_1^{(\lambda)}\gamma_1^{(\lambda')} - 2B\gamma_1^{(\lambda)}\gamma_2^{(\lambda)}\gamma_1^{(\lambda')}\gamma_2^{(\lambda')}W^{(\lambda)}}, \tag{A13}$$

where

$$\begin{aligned} W^{(\lambda)} &= w^{(\lambda)}/2B \\ &= c_{(\lambda)}^5c_{(\lambda')}^5\Bigg\{B[(s + a^{(\lambda')}Ac_{(\lambda')}^3) - 2A^2c_{(\lambda)}^3c_{(\lambda')}^3\gamma_1^{(\lambda)}] \\ &\quad + A\alpha_2q^2\left(\frac{c_{(\lambda')}}{c_{(\lambda)}} + \frac{c_{(\lambda)}}{c_{(\lambda')}}\right) + 2A^2Bc_{(\lambda)}^3c_{(\lambda')}^3\frac{c_{(\lambda)}}{c_{(\lambda')}}\gamma_1^{(\lambda)}\gamma_2^{(\lambda)}\Bigg\}, \end{aligned} \tag{A14}$$

with continued fractions defined as the following:

$$\begin{aligned} \gamma_1^{(\lambda)} &= \frac{1}{s + a^{(\lambda)}Ac_{(\lambda)}^3 + \alpha_2c_{(\lambda)}^2q^2\gamma_2^{(\lambda)}} \\ &= \cfrac{1}{s + a^{(\lambda)}Ac_{(\lambda)}^3 + \cfrac{\alpha_2c_{(\lambda)}^2q^2}{s + 1/\tau_{\mathrm{R}}^{(\lambda)} + a^{(\lambda)}Bc_{(\lambda)}^5 + \cfrac{\alpha_3c_{(\lambda)}^2q^2}{s + 1/\tau^{(\lambda)} + \cdots}}} \end{aligned}$$

$$\begin{aligned} \gamma_2^{(\lambda)} &= \frac{1}{s + 1/\tau_{\mathrm{R}}^{(\lambda)} + a^{(\lambda)}Bc_{(\lambda)}^5 + \alpha_3c_{(\lambda)}^2q^2\gamma_3} \\ &= \cfrac{1}{s + 1/\tau_{\mathrm{R}}^{(\lambda)} + a^{(\lambda)}Bc_{(\lambda)}^5 + \cfrac{\alpha_3c_{(\lambda)}^2q^2}{s + 1/\tau^{(\lambda)} + \cfrac{\alpha_4c_{(\lambda)}^2q^2}{s + 1/\tau^{(\lambda)} + \cdots}}} \end{aligned}$$

$$\begin{aligned} \gamma_3^{(\lambda)} &= \frac{1}{s + 1/\tau^{(\lambda)} + \alpha_4c_{(\lambda)}^2q^2\gamma_4} \\ &= \cfrac{1}{s + 1/\tau^{(\lambda)} + \cfrac{\alpha_4c_{(\lambda)}^2q^2}{s + 1/\tau^{(\lambda)} + \cfrac{\alpha_5c_{(\lambda)}^2q^2}{s + 1/\tau^{(\lambda)} + \cdots}}} \end{aligned}$$

$$\vdots$$

$$\gamma_i^{(\lambda)} = \frac{1}{s + 1/\tau^{(\lambda)} + \alpha_{i+1}c_{(\lambda)}^2q^2\gamma_{i+1}^{(\lambda)}} \quad (i \geq 3),$$

where $a^{(l)} = 2$ and $a^{(t)} = 1$. In Eqs. (A13) and (A14), $(\lambda, \lambda') = (l,t)$ or (t,l).

As a check, letting B be zero, Eq. (A13) reduces to a form as

$$S^{(\lambda)}(q,s) \propto \frac{1/\gamma_1^{(\lambda')}}{(1/\gamma_1^{(\lambda)})(1/\gamma_1^{(\lambda')}) - (Ac_{(\lambda)})(2Ac_{(\lambda')})},$$

which is a coupled-oscillator spectrum as one employed by Barker and Hopfield.[28]

The total spectrum for the considered model is given by the linear combination of the component spectra, viz.,

$$S_{\text{total}}(q,s) = p_1 S^{(l)}(q,s) + p_2 S^{(t)}(q,s),$$

which was employed in the analysis presented in Ref. 50. Since each of $S^{(l)}$ and $S^{(t)}$ contains the normal modes corresponding to the second sound and Mountain mode the total spectrum is still composed of these two normal-mode spectra (S_l and S_2) as those systematically shown in Fig. 5.

APPENDIX B: LINE SHAPE IN THE BALLISTIC LIMIT (Kn$\rightarrow\infty$)

In the ballistic limit, where Kn$\rightarrow\infty$, we obtain that $\boldsymbol{A}=\boldsymbol{A}'=0$. Hence the linear system Eq. (A1) can be reduced to two independent systems, namely, Eqs. (A2) and (A3). As shown in Fig. 4 for Kn=1000, the spectrum in the ballistic limit becomes a round-shaped comb with N sharp peaks, where $N=n_{\max}$ is the number of moments in the ET equation.

The peak positions of the comblike spectrum are obtained by setting the denominator of the spectral function of Eqs. (A4) and (A5), namely, $\det \boldsymbol{L}_N$ or $\det \boldsymbol{T}_N$, to be zero. For a large integer i such that $\alpha_i \simeq 1/4$, these determinants satisfy the following recursive relations:

$$\det \boldsymbol{L}_i = s \det \boldsymbol{L}_{i-1} + \frac{1}{4} c_{(l)}^2 q^2 \det \boldsymbol{L}_{i-2}, \tag{B1}$$

$$\det \boldsymbol{T}_i = s \det \boldsymbol{T}_{i-1} + \frac{1}{4} c_{(t)}^2 q^2 \det \boldsymbol{T}_{i-2}. \tag{B2}$$

We assume that the frequency shift of the ith tooth out of N tooth of the comb is located at

$$\omega_N^{(\lambda)}(i) = c_{(\lambda)} q \cos \phi_N^{(\lambda)}(i), \tag{B3}$$

where (λ) denotes the mode index, (l) or (t), i is an integer $(i=1,2,\ldots,N)$, and $\phi^{(\lambda)}(i)$'s are angles, which are measured counterclockwise from the horizontal axis. Since $\omega_N^{(\lambda)}(i)$ is the ith real root of the dispersion relations in the (ω,q) space, substituting

$$s = i c_{(\lambda)} q \cos \phi_N^{(\lambda)}(i) \tag{B4}$$

into the recursive relations Eqs. (B1) and (B2) gives that

$$\det \boldsymbol{L}_N = \frac{i c_{(l)}^2 q^2}{4} \frac{\sin(N+1)\phi_N^{(l)}}{\cos \phi_N^{(l)}},$$

$$\det \boldsymbol{T}_N = \frac{i c_{(t)}^2 q^2}{4} \frac{\sin(N+1)\phi_N^{(t)}}{\cos \phi_N^{(t)}}.$$

Setting these equal to zero (dispersion relation) shows that the angles $\phi_N^{(\lambda)}$ should satisfy that

$$\phi_N^{(\lambda)}(i) = i \times \frac{\pi}{N+1}. \tag{B5}$$

Equations (B3) and (B5) show that the positions of the comb teeth coincide with the feet of the perpendicular to the ω axis from N points that are equiangularly located $[\Delta\phi=\pi/(N+1)]$ on a half circle of radius $c_{(\lambda)}q$ (see Fig. 12).

The envelope function for the round-shaped comb spectrum can be obtained from the asymptotic expressions for $\gamma^{(l)}$ and $\gamma^{(t)}$. Since all the diagonal elements in $\boldsymbol{L}$ and $\boldsymbol{T}$ are equal to s in this case, we find that

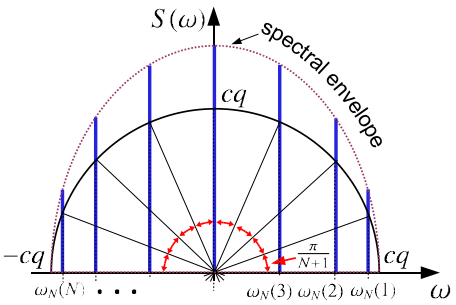

FIG. 12. (Color online) Determination of the frequency shifts and the envelope function for the peaks of the round-shaped comb spectrum when Kn$\gg$1. Here $N=7$ is assumed for visual clarity although the number is actually too small for the approximation presented in the text to be valid.

$$\gamma_\infty(s) = \frac{2}{c^2 q^2}[-s + \sqrt{s^2 + c^2 q^2}] = -\frac{2i}{cq} e^{i\phi_N(i)}, \tag{B6}$$

where we have dropped the mode suffix, and we have substituted the expression of s in Eq. (B4) because the teeth of the comb are located at $\omega_N(i)=cq\cos\phi_N(i)$. Hence the spectra in (ω,q) space are obtained by taking the real parts of Eq. (B6) as

$$\gamma_\infty = \frac{2}{cq} \sin \phi_N(i), \tag{B7}$$

Thus, we see that the spectrum in the ballistic limit has an elliptic envelope.

From Eqs. (B3) and (B7) for the frequency shifts and the envelope, respectively, we see that the spectrum in the ballistic limit for a *finite* number of N is a "sine-weighted" and "cosine-intervaled" comblike spectrum that can be expressed as

$$S_{\text{bal}}(\omega,q,N) \propto \sum_{i=1}^{N} \sin \phi_N(i) \delta[\omega - cq \cos \phi_N(i)], \tag{B8}$$

where the teeth of the comb have been expressed as a sum of sine-weighted delta functions with cosine-intervaled frequency shifts.

Equation (B8) is considered to be an approximated expression for the round-shaped, comblike spectra shown in Fig. 4 for large values of Kn and for a large *but finite* number of moments, namely, $N=30$ or 300 without the asymptotic expression. We have recently suggested[36] that the limiting spectrum when Kn$\rightarrow\infty$ be a half ellipse as Eq. (B8) from analyses with finite numbers of moments, viz., $N\leq 20$. But, it is not true for an infinite number of moments as we will show below.

Now let us examine the limiting line shape for an *infinite* number of moments, viz., when $N\rightarrow\infty$. To do so, we just replace the sum in Eq. (B8) with an integral after introducing an appropriate normalizing factor

$$\lim_{\tau,N\to\infty} S_{bal}(q,\omega) = cq\int_0^\pi \sin\phi\,\delta[\omega - cq\cos\phi]d\phi$$

$$= cq\int_0^\pi \sin\phi\frac{\delta[\omega/cq - \cos\phi]}{|cq|}d\phi$$

$$= \int_0^\pi \sin\phi\frac{\delta[\phi - \arccos(\omega/cq)]}{|\sin[\arccos(\omega/cq)]|}d\phi \tag{B9}$$

$$= \begin{cases} 1 & (|\omega| < cq) \\ \frac{1}{2} & (\omega = \pm cq) \\ 0 & (|\omega| > cq) \end{cases} \tag{B10}$$

$$= \mathrm{rect}\left(\frac{\omega}{2cq}\right), \tag{B11}$$

where the normalizing factor $c^2q^2/2$ has been chosen such that the height at $\omega=0$ is 1. Equation (B11) is a rectangular function, which is nonzero only for the interval $[-cq,cq]$.

A rectangular function can be regarded as a transfer function of an ideal low-pass filter as well known in signal processing. Since an ideal low-pass filter is expected in an infinite ladder-type electric circuit, and since a formal correspondence exists between the ET system and a ladder-type circuit,[66,67] the rectangular spectrum obtained here seems to be quite natural for the linear system of ET with infinite number of moments.

Instead of assuming a delta function for a tooth of the comb spectrum in Fig. 12, it may be assumed that the comb teeth have a finite but very narrow linewidth such that $1/\tau \ll \omega_N(i)$, where τ is the phonon relaxation time defined in Eq. (11). Replacing the delta function in Eq. (B9) with a Lorentzian with a width of $1/\tau$, we obtain a complex susceptibility as

$$\chi(q,\omega) = Ccq\int_0^\pi \sin\phi\frac{1}{\omega - cq\cos\phi - i/\tau}d\phi, \tag{B12}$$

where C is a constant. The real and imaginary parts of $\chi(q,\omega)$ are calculated, respectively, as

$$\mathrm{Re}[\chi(q,\omega)] = Ccq\int_0^\pi \sin\phi\frac{\omega - cq\cos\phi}{(\omega - cq\cos\phi)^2 + 1/\tau^2}d\phi$$

$$= C\int_{\omega\tau - cq\tau}^{\omega\tau + cq\tau}\frac{t}{t^2+1}dt$$

$$= \frac{C}{2}\{\ln[(\omega+cq)^2\tau^2+1] - \ln[(\omega-cq)^2\tau^2+1]\}$$

$$= \frac{C}{2}\ln\frac{(\omega+cq)^2+1/\tau^2}{(\omega-cq)^2+1/\tau^2}, \tag{B13}$$

and

$$\mathrm{Im}[\chi(q,\omega)] = Ccq\int_0^\pi \sin\phi\frac{1/\tau}{(\omega - cq\cos\phi)^2 + 1/\tau^2}d\phi$$

$$= C\int_{\omega\tau - cq\tau}^{\omega\tau + cq\tau}\frac{1}{t^2+1}dt$$

$$= \frac{C}{2}[\tan^{-1}(\omega+cq)\tau - \tan^{-1}(\omega-cq)\tau]. \tag{B14}$$

It is easy to show that, in the ballistic limit ($cq\tau\to\infty$), the right-hand sides of Eqs. (B13) and (B14), respectively, become the following forms:

$$\mathrm{Re}[\chi(q,\omega)]|_{cq\tau\gg1} = C\ln\left|\frac{\omega+cq}{\omega-cq}\right|$$

$$\mathrm{Im}[\chi(q,\omega)]|_{cq\tau\gg1} = C\,\mathrm{rect}\left(\frac{\omega}{2cq}\right).$$

Although we have assumed ballistic regime, it is interesting to investigate the case of hydrodynamic regime. Assuming that $cq\tau\ll1$ in Eqs. (B13) and (B14), we see that

$$\mathrm{Re}[\chi(q,\omega)]|_{cq\tau\ll1} = C\frac{\omega}{\omega^2+1/\tau^2},$$

$$\mathrm{Im}[\chi(q,\omega)]|_{cq\tau\ll1} = C\frac{1/\tau}{\omega^2+1/\tau^2},$$

which are the real and imaginary parts of a central Lorentzian with a width of $1/\tau$. Such a central Lorentzian is expected for $S_2(q,\omega)$ defined in Eq. (24). In fact, this is consistent with the result obtained from Eq. (24) if we assume that $cq\tau\ll1$. Therefore, the expression of the right-hand side of Eq. (B14) can be employed not only in the ballistic regime but also in the hydrodynamic regime as an expression for $S_2(q,\omega)$. Although a slight difference is expected between the exact form [Eq. (24)] and the approximate one [Eq. (B14)] in the intermediate regime, we may reasonably adopt the expressions as in the right-hand side of Eq. (B14) as regime-independent spectral formula for $S_2(q,\omega)$.

[1] C. Kittel, *Quantum Theory of Solids* (Wiley, New York, 1963).
[2] N. W. Ashcroft and N. Mermin, *Solid State Physics* (Thomson Learning, London, 1976).
[3] E. M. Lifshitz and L. P. Pitaevskii, *Physical Kinetics* (Butterworth Heinemann, Oxford, 1981).
[4] C. Kittel, *Introduction to Solid State Physics* (Wiley, New York, 1953).
[5] I. Müller and T. Ruggeri, *Rational Extended Thermodynamics*, 2nd ed. (Springer, Berlin, 1998).
[6] D. Jou, J. Casas-Vázquez, and G. Lebon, *Extended Irreversible Thermodynamics*, 3rd ed. (Springer, Berlin, 2001).
[7] A. Koreeda, T. Nagano, S. Ohno, and S. Saikan, Phys. Rev. B **73**, 024303 (2006).
[8] B. Hehlen, A.-L. Pérou, E. Courtens, and R. Vacher, Phys. Rev. Lett. **75**, 2416 (1995).
[9] V. L. Gurevich and A. K. Tagantsev, Sov. Phys. JETP **67**, 206 (1988).
[10] R. A. Guyer and J. A. Krumhansl, Phys. Rev. **148**, 778 (1966).
[11] T. Schneider and E. Stoll, Phys. Rev. B **17**, 1302 (1978).
[12] T. Schneider and E. Stoll, Phys. Rev. B **18**, 6468 (1978).
[13] D. W. Pohl and V. Irniger, Phys. Rev. Lett. **36**, 480 (1976).
[14] W. Dreyer and H. Struchtrup, Continuum Mech. Thermodyn. **5**, 3 (1993).
[15] J. Callaway, Phys. Rev. **113**, 1046 (1959).
[16] C. Herring, Phys. Rev. **95**, 954 (1954).
[17] L. D. Landau and E. M. Lifshitz, *Electrodynamics of Continuous Media* (Pergamon, Amsterdam, 1984).
[18] R. K. Wehner and R. Klein, Physica (Utrecht) **62**, 161 (1972).
[19] R. Klein, *Nonequilibrium Phonon Dynamics* (Plenum, New York, 1985).
[20] C. C. Ackerman, B. Bertman, H. A. Fairbank, and R. A. Guyer, Phys. Rev. Lett. **16**, 789 (1966).
[21] C. C. Ackerman and W. C. Overton, Phys. Rev. Lett. **22**, 764 (1969).
[22] T. F. McNelly, S. J. Rogers, D. J. Channin, R. J. Rollefson, W. M. Goubau, G. E. Schmidt, J. A. Krumhansl, and R. O. Pohl, Phys. Rev. Lett. **24**, 100 (1970).
[23] H. E. Jackson, C. T. Walker, and T. F. McNelly, Phys. Rev. Lett. **25**, 26 (1970).
[24] H. E. Jackson and C. T. Walker, Phys. Rev. B **3**, 1428 (1971).
[25] It is assumed that $\tau_R^{(\lambda)} \to \infty$ and $\tau_N^{(\lambda)} \to 0$.
[26] J. A. Sussmann and A. Thellung, Proc. Phys. Soc. London **81**, 1122 (1963).
[27] H. Beck and R. Beck, Phys. Rev. B **8**, 1669 (1973).
[28] A. S. Barker and J. J. Hopfield, Phys. Rev. **135**, A1732 (1964).
[29] R. D. Mountain, J. Res. Natl. Bur. Stand. **70A**, 207 (1966).
[30] The modification to the frequency and linewidth of the second sound is minimal for $n_{\max}=2$ as we have seen above. However, if we set $n_{\max}$ to be 3, Eqs. (31) and (32) give more complicated renormalization to the second-sound frequency and linewidth. Note that Eqs. (31) and (32) in the hydrodynamic regime are approximated to give the imaginary and real parts of a Lorentzian, respectively, so that $\gamma_3(q,\omega)=\tau/(1+i\omega\tau)$ (for $n_{\max}=3, cq\tau \ll 1$). This result can be understood that the self-energy for the second-sound propagator can be approximated as a Lorentzian in thermodynamic limit or that the memory function of the viscosity in a phonon gas can be approximated as an exponential function in the Markovian regime.
[31] H. Beck, P. F. Meier, and A. Thellung, Phys. Status Solidi A **24**, 11 (1974).
[32] G. J. Coombs and R. A. Cowley, J. Phys. C **6**, 121 (1973).
[33] R. A. Field, D. A. Gallagher, and M. V. Klein, Phys. Rev. B **18**, 2995 (1978).
[34] G. Eckold, K. Funke, J. Kalus, and R. E. Lechner, J. Phys. Chem. Solids **37**, 1097 (1976).
[35] J. R. Sandercock, *Light Scattering in Solids* (Springer-Verlag, Berlin, 1982), Vol. III, Chap. 6.
[36] A. Koreeda and S. Saikan, Ferroelectrics **347**, 12 (2007).
[37] W. Hayes and R. Loudon, *Scattering of Light by Crystals* (Wiley, New York, 1978).
[38] E. Farhi, A. K. Tagantsev, B. Hehlen, R. Currat, L. A. Boatner, and E. Courtens, Physica B **276-278**, 274 (2000).
[39] E. Farhi, Ph.D. thesis, Université Montpellier II, 1998.
[40] K. B. Lyons and P. A. Fleury, Phys. Rev. Lett. **37**, 161 (1976).
[41] M. W. Anderson, S. M. Lindsay, and R. T. Harley, J. Phys. C **17**, 6877 (1984).
[42] A. Koreeda, M. Yoshizawa, S. Saikan, and M. Grimsditch, Phys. Rev. B **60**, 12730 (1999).
[43] Two-phonon difference process from different phonon dispersion is also possible in general. In such a case, the two-phonon-dispersion curves must be close at a point in the Brillouin zone. In practical system, such points are usually located at the edges of the Brillouin zone, where phonon dispersions are usually flat. From such flat portion of the phonon dispersion, however, TPDS predicts a rather narrow central peak, which is not consistent with the observed spectra.
[44] The pair width should be $1/\tau$ because it is physically identical with the mean rate of collision between phonons.
[45] In Ref. 42, we have just replaced the delta function $\delta[\omega - cq\cos\phi]$ with $\delta[\phi - \arccos(\omega/cq)]$, but it was mathematically incorrect: the correct calculation is presented in Eq. (B9).
[46] R. Klein, *Anharmonic Lattices, Structural Transitions and Melting* (Noordhoff, Leiden, 1974).
[47] E. Farhi, A. K. Tagantsev, B. Hehlen, R. Currat, L. A. Boatner, and E. Courtens, Ferroelectrics **239**, 25 (2000).
[48] J. R. Sandercock, Solid State Commun. **26**, 547 (1978).
[49] H. E. Jackson, R. T. Harley, S. M. Lindsay, and M. W. Anderson, Phys. Rev. Lett. **54**, 459 (1985).
[50] A. Koreeda, R. Takano, and S. Saikan, Phys. Rev. Lett. **99**, 265502 (2007).
[51] *Thermophysical Properties of Matter: The TPRC Data Series*, edited by Y. S. Touloukian (IFI, New York/Plenum, New York, 1970), Vol. 2.
[52] *Thermophysical Properties of Matter: The TPRC Data Series*, edited by Y. S. Touloukian (IFI, New York/Plenum, New York, 1970), Vol. 5.
[53] J. D. Axe, J. Harada, and G. Shirane, Phys. Rev. B **1**, 1227 (1970).
[54] J. H. Barrett, Phys. Rev. **86**, 118 (1952).
[55] E. Courtens, B. Hehlen, G. Coddens, and B. Hennion, Physica B (Amsterdam) **219-220**, 577 (1996).
[56] A. Koreeda and S. Saikan, J. Phys.: Conf. Ser. **92**, 012176 (2007).
[57] J. Scott and H. Ledbetter, Z. Phys. B: Condens. Matter **104**, 635 (1997).
[58] E. Courtens, B. Hehlen, E. Farhi, and A. Tagantsev, Z. Phys. B: Condens. Matter **104**, 641 (1997).
[59] J. F. Scott, A. Chen, and H. Ledbetter, J. Phys. Chem. Solids **61**, 185 (2000).

[60] M. Tan, Y. Tsujimi, and T. Yagi, J. Korean Phys. Soc. **46**, 97 (2005).
[61] K. A. Müller and H. Burkard, Phys. Rev. B **19**, 3593 (1979).
[62] Y. Tsujimi and M. Itoh, Ferroelectrics **355**, 61 (2007).
[63] H. Taniguchi, M. Takesada, M. Itoh, and T. Yagi, J. Phys. Soc. Jpn. **73**, 3262 (2004).
[64] H. Taniguchi, T. Yagi, M. Takesada, and M. Itoh, Phys. Rev. B **72**, 064111 (2005).
[65] E. Farhi, A. K. Tagantsev, R. Currat, B. Hehlen, E. Courtens, and L. A. Boatner, Eur. Phys. J. B **15**, 615 (2000).
[66] R. Unbehauen, Electr. Eng. **88**, 343 (2006).
[67] S. H. Yoon, Eur. J. Phys. **28**, 277 (2007).